universität
wien

DIPLOMARBEIT

A mathematical model for the evolution of division of labor in an explicit ecological context

angestrebter akademischer Grad

Magistra der Naturwissenschaften (Mag^a. rer. nat.)

Verfasser:	Helene Camilla Weigang
Matrikel-Nummer:	0606898
Studienrichtung:	Mathematik
Betreuer:	Dr.Claus Rüffler

Wien, August 2011

Danksagung

Ein herzlicher Dank gilt meinem Betreuer Dr.Claus Rüffler dessen Unterstützung und Verfügbarkeit weit über die Pflichten eines Diplomarbeitsbetreuers hinaus gingen. Weiters bedanke ich mich bei Prof.Dr.Joachim Hermisson für hilfreiche Kommentare und Anmerkungen.
Ein Dankeschön gilt Hannes Svardal für seine Hilfe beim Programmieren. Weiters danke ich meiner Familie die mich immer unterstützt hat und mir mein Leben dadurch erleichtert hat. Nicht zuletzt danke ich Peter Bednarik für erfrischende Kaffeepausen und dass er stets ein offenes Ohr für mich hat.

Abstract

In nature different patterns of resource consumption evolved in response to an enormous variety of resources. In individuals with modular structures, where the phenotypes of the modules determine the success in resource consumption, three forms can be distinguished. First, generalists, that consist of identical modules that are equally adapted to the resources, second, specialists that consist of identical but specialized modules for one resource and third, organisms with functional differentiated modules, such that each module is specialized for a different resource, a phenomenon called division of labor.

Here, I combine these three evolutionary outcomes in a single analysis. I analyze an one-consumer two-resources model where consumers are characterized by two ancestrally undifferentiated modules, both contributing to resource consumption. The potential of modules to contribute to one resource is assumed to go at the expense of specialization on the other resource (such trade-off is described by trade-off curves). With the methods of Adaptive Dynamics and Critical Function Analysis I find that (*i*) convex trade-offs, (*ii*) negative interaction between modules as well as (*iii*) positional effects (asymmetries in the contribution of each module for the resources) favor the evolution of division of labor. Furthermore, positive interaction between modules and convex trade-offs can lead to evolutionary branching (a change from a monomorphic to a dimorphic population). Moreover, the model is studied by means of individual-based simulations to illustrate the robustness of the analytical results. Furthermore, I find that populations with functional specialized modules do not undergo evolutionary branching.

Deutsche Zusammenfassung

Auf Grund von unterschiedlichen Nahrungsquellen haben Organismen verschiedenste Arten des Nahrungserwerbs entwickelt. Individuen die aus einzelnen Segmenten bestehen haben sich verschiedenartig auf Nahrungserwerb spezialisiert. Es gibt Generalisten, welche aus identen Segmenten oder Modulen bestehen die gleich gut für alle vorkommenden Ressourcen angepasst sind, Spezialisten, deren idente Module für eine Ressource spezialisiert sind und Organismen mit funktionell differenzierten Modulen. Je ein Modul der letzteren Organismen ist auf nur eine bestimmte Ressource spezialisiert. Diese Art der Spezialisierung wird Arbeitsteilung genannt.

In dieser Arbeit werden die drei Möglichkeiten der Spezialisierung unterschieden und in einem ein-Konsument zwei-Ressourcen Modell analysiert. Konsumenten sind durch zwei, ursprünglich, undifferenzierte Module gekennzeichnet, welche sich auf zwei Ressourcen spezialisieren können. Es wird angenommen, dass eine Spezialisierung auf eine Ressource zu Lasten der Spezialisierung für die andere geht (daraus resultiert ein Trade-Off). In diesem Modell, welches ich durch Hilfe von 'Adaptive Dynamics' und 'Critical Function Analysis' analysiert habe, geht hervor, dass (*i*) ein konvexer Trade-Off, (*ii*) negative Interaktion zwischen den Modulen und (*iii*) positionale Effekte, welche als Asymmetrien in der Ressourcenkonsumation beschrieben werden knnen, Arbeitsteilung fördern. Darüber hinaus, wird evolutionäres 'Branching', was die Aufspaltung von einer in zwei Populationen bedeutet, gefördert wenn sich Module gegenseitig positiv beeinflussen und Trade-Offs konvex sind. Des weiteren, habe ich Individuen-basierte Simulationen durchgeführt, um die Stabilität der analytischen Resultate zu überprüfen. Weiters komme ich zu dem Ergebnis, dass Populationen nicht polymorph werden, wenn sie arbeitsteilende Module ausgebildet haben.

Contents

Chapter 1

Introduction

Planet Earth is filled with an immense number of organisms showing a tremendous diversity of specialization patterns. Specialization is a common process and can occur at two different levels: First, specialization among related species or among populations exists. It varies widely and is generating phenotypic variation. For example, sticklebacks (*Gasterosteus sp.*) are specialized for different ecological environments. Stickleback species are adapted diversely and became morphologically distinct, measured in terms of body size as well as body shape (Schluter, 1995), to exploit different resources. Cisne (1974) documents an example of specialization in aquatic free-living arthropods. These species of the phylum Arthropoda have specialized specific limb pairs for specific sets of functions. In going from primitive to advanced groups of this phylum, more and more limb pairs are specialized. Most primitive extinct forms of this phylum are represented by trilobites where postoral head and trunk limbs serve in feeding and locomotion, respectively. The limbs of these forms take on a broad set of functions. The cephalocarid crustaceans (e.g. *Hutchinsoniella*) have more differentiated limbs for more specialized functions. The anterior postantennal limbs serve to handle food, to comminute it and to stuff it into the mouth. Additionally, the cephalocarids have adapted posterior head and trunk limbs which are adapted to perform functions such as locomotion and food collection (Cisne, 1974).

Second, specialization can occur in organisms with iterated structures that can be decomposed into modules. Modularity can facilitate adaptation and functional specialization and can lead to evolutionary innovations (Espinosa-Soto and Wagner, 2010) such as, e.g., division of labor. Division of labor occurred when organisms have functionally specialized and functionally differentiated modules, each module specialized for a peculiar task. The iterated modules can be genes, cells, teeth, limbs or highly related individuals in colonial organisms. A well known example of division of labor is

the cellular dichotomy in the green algae *Volvox carteri*. *Volvox carteri* show a pattern of differentiation between two cell types that serve specific functions. The algae consist of a set of non-motile cells, called gonidia, which are specialized for asexual reproduction while the somatic cells execute vegetative and non-reproductive functions (Kirk, 2005). Another example can be found in the Hydrozoa which are usually colonial, with multiple polyps connected together. The hydrozoa *Obelia geniculata* show division of labor with some polyps specialized for feeding and others for reproduction (Campbell, 1997). Many eusocial insects, such as leaf-cutter ants exhibit task-related division of labor (Wilson, 1980), where individuals specialize on performing a particular task in a colony. Furthermore, division of labor evolved in the dental adaptation for food processing in mammalia (Butler, 1983).

But how did division of labor evolve? Rueffler and Wagner (in rev.) looked at an optimality model of division of labor and present a unifying perspective for the evolution of functional specialization of modules. In this work, Rueffler and Wagner (in rev.) identify conditions that favor division of labor. In their model modules contribute to two different biological tasks and the potential of modules to contribute to these tasks is traded off. Their work is based on the assumptions that the modules where ancestrally undifferentiated and that the fitness of an organism increases with increasing levels of contribution to a task. The contribution of a module to a task is measured in performance. With making these assumptions, they identify three factors that favor division of labor: (*i*) positional effects, which means that the contribution of tasks is affected differently because of the position within an organism, (*ii*) accelerating performance functions and (*iii*) negative interaction of modules, which means that modules are affecting each other negatively so that the sum of their separate contribution is higher than their joint contribution.

In nature, survival of an organism also depends on the environment it experiences and in turn, the environmental conditions are determined by the organism itself. Any living individual is occupying a specific ecological habitat or niche and makes use of the abundant abiotic and biotic resources. The myriads of lifeforms compete for sunlight, nutrients, water, shelter or simply for space. Three different resource utilization patterns evolved. First, generalists, which thrive in various environmental conditions and are adapted to a wide range of resources and therefore can elude to other abundant resources if the most consumed one is scarce, second, specialists that tolerate only restricted environmental conditions and are specialized for a narrow range of resources with morphologically adapted structures (Campbell, 1997) that do not differ in form or function. Division of labor in the context of resource

[1] http://www.uh.edu/engines/epi1948.htm

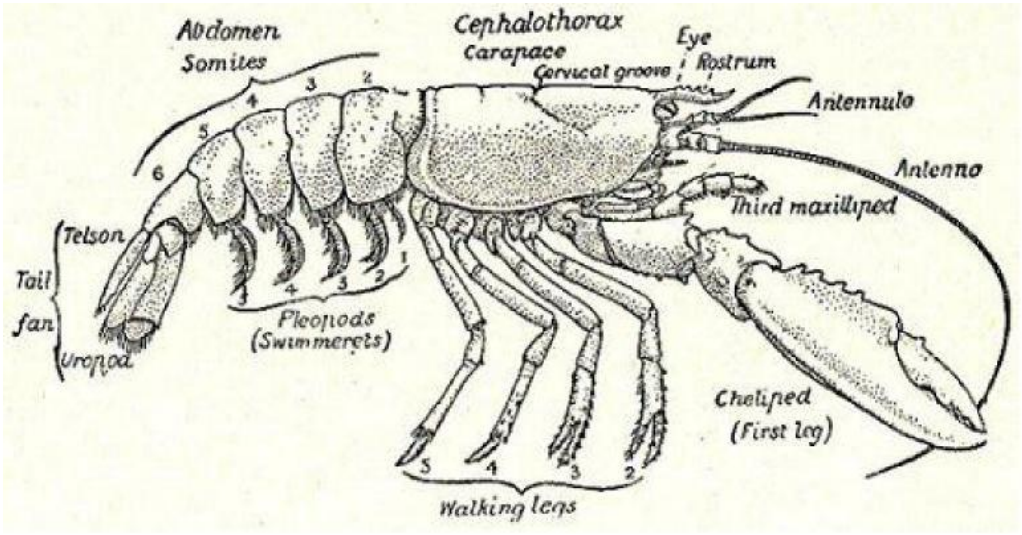

Figure 1.1: External anatomy of a lobster (Figure from web page[1])

consumption occurs when individuals have each module specialized for a different resource. A relevant example is presented in the work of Cisne (1974). Division of labor evolved in lobster of the genus *Homarus*. They have evolved functional specialized and morphological differentiated pairs of limbs, which serve to feed on specific resources. Lobsters have limbs specialized for feeding on large food items in addition to limbs adapted to feed on items in suspension (see Figure 1.1). Behind their two pairs of antennae, they have six morphologically varying limb pairs which serve for a multitude of functions: the collection of food and the breakdown for ingestion (see Figure 1.2). Moreover they have the large pair of chelate limbs and four pairs of walking legs. The first two pairs of walking legs have claws which are almost used as hands to handle food and manipulate objects including large food items (see Figure 1.1). Furthermore, lobster have specialized trunk limbs for walking, swimming, respiration, copulation and brooding (Cisne, 1974).

Once one takes the feedback between a consumer and in particular resource consumption into account it raises the question if division of labor evolves alternatively to a generalist or specialist strategy. I designed a one-consumer two-resource model that incorporates density-dependent and frequency-dependent selection. I analyze whether or not division of labor evolves in this specific ecological scenario and if functional differentiation occurs as an alternative to evolutionary branching. I simply ignore the importance of genes and sex and limit the model to phenotypic evolution under clonal reproduction. Understanding the mechanism of evolutionary diversi-

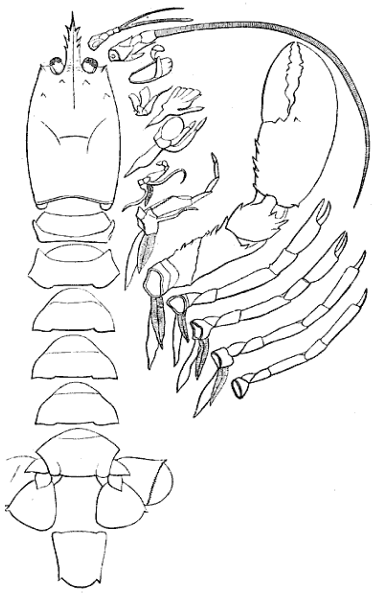

Figure 1.2: External cephalothorax features of a lobster (Figure from web page [2])

fication of consumers turns out to be an interesting and surprisingly quite unexamined problem in evolutionary ecology and the spectrum of possible dynamical behavior becomes a lot richer when an eco-evolutionary feedback is taken into account and environmental conditions co-evolve. When evolutionary and ecological dynamics occur on an similar timescale, this may lead to very complex dynamics. With the aid of Adaptive Dynamics and Critical Function Analysis I analyzed my eco-evolutionary model.

In the next Sections 1.1 and 1.2 I give an overview of the mathematical methods used to analyze the model. Chapter 2 presents the eco-evolutionary model. In chapter 3 and chapter 4 analytical, numerical and simulation results are presented. Chapter 5 contains the conclusion and discussion.

1.1 Adaptive Dynamics

Adaptive Dynamics is a mathematical framework that relates ecological to evolutionary processes (Dieckmann and Law, 1996; Geritz et al., 1997, 1998; Metz et al., 1992, 1996). It is a toolbox that allows to investigate frequency-dependent selection, using elements of dynamical systems theory, population dynamics and evolutionary game theory. Adaptive Dynamics is an approximation of evolutionary dynamics based on the assumptions that individuals

[2] http://etc.usf.edu/clipart/6900/6925/lobster_6925.htm

of a large population reproduce asexually and that mutations occur infrequently after a resident population has reached its population dynamical equilibrium, i.e., the evolutionary timescale is assumed to be much longer than the ecological timescale. A basic tool in the perspective of Adaptive Dynamics is the concept of invasion fitness. It allows to determine which mutant is a successful invader. The resident types are characterized by a n-dimensional trait vector (also referred to as strategy or phenotype) which I denote by $\boldsymbol{\theta} \in \mathbb{R}^n$, the mutant is characterized by the trait vector $\boldsymbol{\theta'} \in \mathbb{R}^n$. The invasion fitness of a rare mutant $\rho(\boldsymbol{\theta'}, \boldsymbol{\theta})$ in a resident population at equilibrium is defined as its expected long-term exponential growth rate in the environment set up by the resident type (Metz et al., 1992). The rare mutant is similar to the resident from which it originated and initially has a negligible effect on the environment set by the residents. The crucial question is whether or not the mutant can invade the resident. The fitness of the resident in a population is zero after it has reached its equilibrium size since there are no trends in population growth, $\rho(\boldsymbol{\theta}, \boldsymbol{\theta}) = 0$. Resident individuals are selectively neutral among themselves. If $\rho(\boldsymbol{\theta'}, \boldsymbol{\theta}) > 0$, the mutant can increase in frequency. In the opposite case where $\rho(\boldsymbol{\theta'}, \boldsymbol{\theta}) < 0$, the mutant dies out. Even if the mutant's invasion fitness is positive, there is a risk that a mutant will not invade as a result of stochastic extinction. After a succesfull invasion there are two possible scenarios: In the case where the fitness with reversed roles is negative ($\rho(\boldsymbol{\theta}, \boldsymbol{\theta'}) < 0$), the resident cannot recover when rare itself and eventually the mutant becomes fixed in the population (Geritz et al., 1998). Hence, the mutant ousts the resident and a trait substitution occurs with the new resident trait equal to $\boldsymbol{\theta'}$. If both $\rho(\boldsymbol{\theta'}, \boldsymbol{\theta}) > 0$ and $\rho(\boldsymbol{\theta}, \boldsymbol{\theta'}) > 0$, then neither strategy can eliminate the other. A phenotopic dimorphism arises in the population, which means that these two phenotypes coexist.

To see which nearby mutants can invade a resident one has to look at the gradient of the invasion fitness function

$$S_i(\boldsymbol{\theta}) = \frac{\partial \rho(\boldsymbol{\theta'}, \boldsymbol{\theta})}{\partial \theta'_i}\Big|_{\boldsymbol{\theta'}=\boldsymbol{\theta}} \qquad \text{i} \in \{1, 2, \ldots, n\}, \tag{1.1}$$

where θ'_i is the i-th component of the trait vector $\boldsymbol{\theta'}$.

If $S_i(\boldsymbol{\theta}) > 0$ only mutants with $\theta'_i > \theta_i$ can invade, whereas a negative sign ($S_i(\boldsymbol{\theta}) < 0$) signifies that invaders with a trait value smaller than the resident's ($\theta'_i < \theta_i$) can invade (where $\theta'_j = \theta_j$ for $j \neq i$). Directional selection drives the resident strategy to a point where the fitness gradient equals zero (see Figure 1.3). This strategy, $\boldsymbol{\theta}^*$, satisfying

$$S_i(\boldsymbol{\theta}^*) = 0 \qquad \text{for all } i \in \{1, 2, \ldots, n\}, \tag{1.2}$$

is called **evolutionary singular strategy** (Geritz et al., 1998).

Considering singular points one has to clarify two questions: First, is

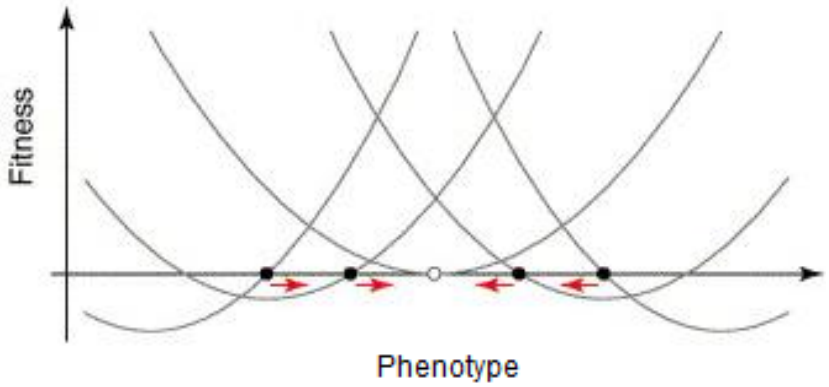

Figure 1.3: Convergence stable fitness minimum. Selection drives the phenotype to the singular strategy, but once it is there it resides at a fitness minimum (Figure from Rueffler et al. (2006a)).

the singular strategy a fitness minimum or maximum? Second, will the population approach the singular strategy by the evolutionary process? One can determine these two properties in the one-dimensional trait space at singular points algebraically and graphically.

The algebraic conditions for these two properties of singular points are (Geritz et al., 1997, 1998):

1. A singular strategy θ^* is locally evolutionary stable strategy (**ESS**) if no mutant with a nearby strategy exists that is successful. The singular point is a maximum of the fitness function. In other words, no mutant can invade and $\rho(\theta', \theta^*) < 0$ for all $\theta' \neq \theta^*$ in the neighborhood of θ^*. Thus,

$$\frac{\partial^2 \rho(\theta', \theta^*)}{\partial \theta'^2}\Big|_{\theta'=\theta^*} < 0. \tag{1.3}$$

   An evolutionary stable strategy is an evolutionary trap, which means that once it has become established no further phenotypic change is possible.

   In the opposite case,

$$\frac{\partial^2 \rho(\theta', \theta^*)}{\partial \theta'^2}\Big|_{\theta'=\theta^*} > 0 \tag{1.4}$$

   the singular point is a fitness minimum. Surrounding mutants can invade the resident population.

2. A singular strategy θ^* is (locally) **convergence stable** if a phenotype close to θ^* can be invaded by mutants even closer to θ^*. Put differently,

$\rho(\theta', \theta) > 0$ for nearby mutants that are even closer to the singular point, that is, $\theta < \theta' < \theta^*$ and $\theta > \theta' > \theta^*$. A singular point is convergence stable if and only if

$$\frac{\partial^2 \rho(\theta', \theta)}{\partial \theta'^2}\Big|_{\theta=\theta'=\theta^*} + \frac{\partial^2 \rho(\theta', \theta)}{\partial \theta' \partial \theta}\Big|_{\theta=\theta'=\theta^*} < 0. \tag{1.5}$$

A convergence stable strategy is an evolutionary attractor.

If the singular strategy is not convergence stable, selection drives the population away. The singular point is an evolutionary repellor if and only if

$$\frac{\partial^2 \rho(\theta', \theta)}{\partial \theta'^2}\Big|_{\theta=\theta'=\theta^*} + \frac{\partial^2 \rho(\theta', \theta)}{\partial \theta' \partial \theta}\Big|_{\theta=\theta'=\theta^*} > 0. \tag{1.6}$$

The two properties explained above are mutually independent and can therefore be combined in four different ways each corresponding to different evolutionary scenarios (see Table 1.1):

1. If a singular point is an ESS and convergence stable, then it is called continuously stable strategy or **CSS**. CSSs are final stops of evolution and no diversification occurs.

2. If a singular point is convergence stable and not an ESS, the point is called an evolutionary branching point (**BP**). Nearby strategies experience directional selection towards the singular one. However, due to the fact that it lacks evolutionary stability, evolution does not stop there. At such a point the monomorphic population splits into two diverging subpopulations (see Figure 1.3).

3. If a singular point θ^* is not ESS and not convergence stable, it is a **repellor** of the adaptive dynamics. The population will evolve away from such points.

4. If a singular point is not convergence stable but an ESS it is a **Garden of Eden** point. A population near this point will evolve away and even if a resident population resides at this local fitness maximum it can easily be driven away due to small perturbations.

A convenient way of analyzing the evolutionary dynamics of a monomorphic population graphically, is the use of **pairwise invasibility plots** (PIPs) (see Figure 1.4)(Diekmann, 2004). On the principal diagonal where $\theta' = \theta$ the fitness function is always zero. This diagonal is a borderline where the sign of the fitness function changes. In the PIP there is a second line where the invasion fitness vanishes. Solving $\rho(\theta', \theta) = 0$ for θ' with $\theta' \neq \theta$ gives this second line. Singular points are located at the intersections of

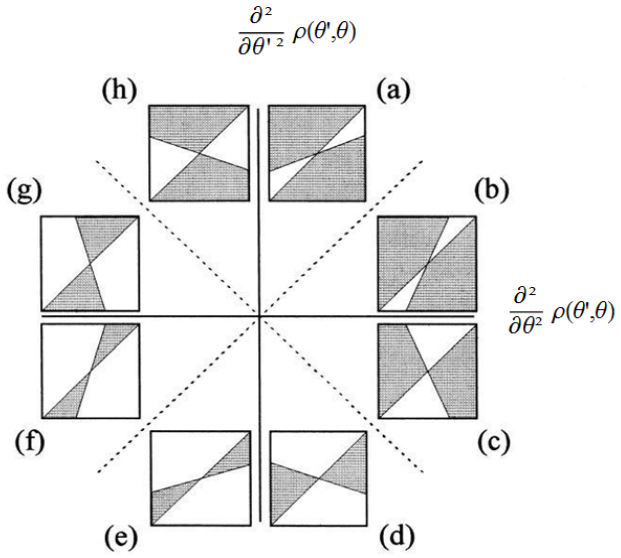

Figure 1.4: Pairwise Invasibility Plots: All possible local configurations of pairwise invasibility plots. It is a contour plot of the sign of the invasion fitness function. Possible strategies of the resident are plotted along the x-axis and mutant strategies along the y-axis. Shaded regions indicate combinations of mutant and resident with $\rho(\theta', \theta) > 0$. White regions indicate combinations where $\rho(\theta', \theta) < 0$. The axes (not the axes of the PIPs) give the relation to the second-order derivatives of the fitness function. Under the x-axis all singular points, located at the intersection of the two lines in each PIP, are ESS (a vertical line in each PIP through the singular point lies within a white region. Along this vertical line the fitness function has a maximum at $\theta' = \theta^*$). Under the hatched main diagonal all singular points are convergence stable (in the PIP there is both a positive region below the diagonal to the right of the singular point and above the diagonal to the left). Above the diagonal in the $-45°$-direction coexistence of two populations is possible (coexisting strategies near a singular strategy are given by the overlapping parts of the shaded regions in the PIP and its mirror image taken along the main diagonal). The plots (a),(g),(h) are the cases where the singular points are repellors, the singular point in (b) refers to a branching point, (c)-(e) give CSS points, and the singular point in plot (f) is a Garden of Eden (Figure from Geritz et al. (1998)).

Table 1.1: Classification of Singular Points in one-dimensional trait spaces. The signs denote whether or not the condition is fulfilled.

		ESS	
		+	−
Convergence Stable	+	CSS	BP
	−	GoE	REP

the main diagonal with the second line. These points are the fitness maxima and minima. The convergence stability and the evolutionary stability criteria can be read from those plots as explained in Figure 1.4.

To extend the criteria from one-dimensional to higher dimensional trait spaces one analyzes the definiteness of the **Hessian matrix** H of the fitness function and the **Jacobian matrix** J of the fitness gradient at the singular point (Leimar, 2005). I follow Leimar (2005) and call a matrix M positive (negative) definite if its symmetric part $(\mathsf{M} + \mathsf{M}^T)/2$ is positive (negative) definite and similarly for indefiniteness. The Hessian matrix determines whether or not a singular point can be invaded by mutants. In the multidimensional case singular points can be hilltops, bottoms of a trough or saddle points of the fitness landscape.

The entries of the Hessian matrix are of the following form:

$$h_{ij} = \frac{\partial^2 \rho(\boldsymbol{\theta}', \boldsymbol{\theta})}{\partial \theta_i' \partial \theta_j'}\Big|_{\boldsymbol{\theta}=\boldsymbol{\theta}'=\boldsymbol{\theta}^*} \qquad \text{for all } i, j \in \{1, 2, \ldots, n\}. \tag{1.7}$$

A singular point is a local fitness maximum if and only if the Hessian is negative definite. On the other hand, a singular point is invadable in all directions if the Hessian matrix is positive definite. Then the singular point is a local minimum. If the matrix H is indefinite the fitness landscape is a saddle point at the singular point. At a local minimum or saddle there exist disruptive selection along some direction in trait space (Leimar, 2009).

Convergence stability in the multidimensional case is difficult to define and one cannot expect a completely general stability criterion.
Nevertheless one can describe the gradual adaptive change of the traits through a sequence of mutant invasions. This dynamics can be described by the **canonical equation** (Dieckmann and Law, 1996):

$$\frac{d}{dt}\theta_i = m(\boldsymbol{\theta}) \sum_j c_{ij}(\boldsymbol{\theta}) S_j(\boldsymbol{\theta}). \tag{1.8}$$

This equation considers natural selection and genetic correlations. The non-negative factor $m(\boldsymbol{\theta})$ is related to the rate of occurrence of mutations. The symmetric matrix $\mathsf{C}(\boldsymbol{\theta})$ stands for the positive definite covariance matrix

that gives the distribution of mutational increments ($c_{ij}(\boldsymbol{\theta})$ are the entries of the matrix) (Dieckmann and Law, 1996; Leimar, 2009). This equation holds for large population sizes and small mutation rates with small effects. If there is no covariance and the mutational variance in the different traits is equal, then the selection gradient provides all information about the direction of evolutionary change. Therefore, the canonical equation or the selection gradient respectively, is a useful starting point to investigate whether trait dynamics approach a singular strategy. Near a singular point $\boldsymbol{\theta}^*$ one can approximate the selection gradient with the Jacobian matrix of the selection gradient in order to analyze convergence stability in terms of properties of this matrix. The Jacobian is the sum of two matrices (Leimar, 2009): $\mathsf{J} = \mathsf{Q} + \mathsf{H}$ where Q is the matrix that consists of second-order partial derivatives of the following from:

$$q_{ij} = \frac{\partial^2 \rho(\boldsymbol{\theta}', \boldsymbol{\theta})}{\partial \theta_i' \partial \theta_j}\Big|_{\boldsymbol{\theta}'=\boldsymbol{\theta}=\boldsymbol{\theta}^*} \qquad \text{for all } i, j \in \{1, 2, \ldots, n\}. \tag{1.9}$$

When the Jacobian is negative definite at the singular point nearby strategies will approach the singular point, for any positive definite covariance matrix C. Such singular points are called **strongly convergence stable** (Leimar, 2009). If J is positive definite the singular point is not convergence stable and thus repelling for any covariance matrix. If J is indefinite, the convergence stability can depend on the covariance matrix C.

Although no complete classification of singular points in multi-dimensional trait spaces exist, a few cases are well understood:

- If J and H are negative definite, the point is strongly convergence stable and locally uninvadable, and thus a (multidimensional) CSS.
- If the Jacobian is negative definite and the Hessian is indefinite or positive definite, then the population undergoes evolutionary branching and splits up into two subsequently phenotypically diverging subpopulations.
- If the Jacobian is indefinite and the Hessian is positive definite at the singular point there might be evolutionary branching depending on the nature of genetic correlations (Leimar, 2005).

1.2 Critical Function Analysis & Invasion Boundaries

'Darwinian demons' (Barton et al., 2007; Kisdi, 2006; Law, 1979) are fictive organisms that maximize all aspects of fitness. They produce an infinite number of offspring, live infinitely long and achieve this in any habitat they encounter. But these hypothetical organisms are not dominating the Earth

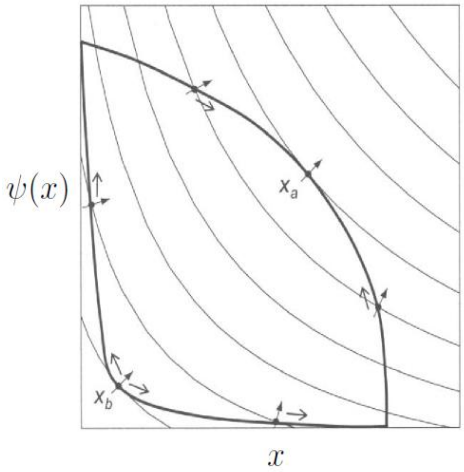

Figure 1.5: Thin lines are critical functions numerically solved for various initial conditions. The solid lines are two trade-off curves, where x_a is a convergence stable strategy because the trade-off is concave and the critical function is convex. The singular point x_b is not convergence stable, since the trade-off curve is more convex then the critical function (Figure from De Mazancourt and Dieckmann (2004)).

because they do not exist. Improvements in some traits result in a decline in others. This phenomenon occurs inevitably in nature and is called **trade-off**. Individuals can only evolve a limited set of feasible trait combinations. The outer boundary of such a set is called **trade-off curve** (Rueffler et al., 2006b) and the shape (concave, linear, convex) of this curve determines the evolutionary outcome. Assuming that the fitness function is increasing for both traits the population will evolve towards the trade-off curve and stays close to the trade-off boundary once it is located there.

However, trade-off curves are extremely difficult to determine empirically and this constitutes a major gap between empirical data and theory. In the following two sections I present methods to predict the propterites of singular points geometrically.

1.2.1 Critical Function Analysis

Critical function analysis is a geometric method that enables predicting frequency-dependent evolutionary outcomes without committing to a particular shape of trade-off curves. It provides a quick and visual way to tell for which shape of trade-off a singular strategy is convergence stable or repelling.

Assume a two dimensional trait space with traits x and y. Furthermore,

trait x and y are traded off such that $\psi(x) = y$, where ψ is a twice continuously differentiable trade-off function. The traits are heritable and the shape of the trade-off curve is not affected by the environment or by the population. With some abuse of notation invasion fitness can be written as:

$$\rho(x', x) = \rho(x', \psi(x'), x, \psi(x)) \tag{1.10}$$

As already described in Section 1.1, singular points can be derived by setting the fitness gradient equals zero:

$$\rho_1(x', \psi(x'), x, \psi(x)) + \rho_2(x', \psi(x'), x, \psi(x))\dot{\psi}(x') = 0 \tag{1.11}$$

where $\rho_1 = \frac{\partial \rho}{\partial x'}$ and $\rho_2 = \frac{\partial \rho}{\partial \psi(x')}$. De Mazancourt and Dieckmann (2004) introduce curves that are orthogonal to the local fitness gradient at the singular strategy, have the slope of the fitness gradient's normal and thus form solutions of the ordinary differential equation

$$\psi'_{cr}(x) = -\frac{\rho_1(x, \psi(x), x, \psi(x))}{\rho_2(x, \psi(x), x, \psi(x))} \tag{1.12}$$

to different initial values (Kisdi, 2006).

The curves that solve equation (1.12) in every point are called **critical functions** (Kisdi, 2006) or A-boundaries (De Mazancourt and Dieckmann, 2004). Singular strategies are those points where the critical functions have the same slope as the trade-off function. Critical functions separate regions of phenotypes where singular points are evolutionary attracting and can get reached through sequences of small and selectively advantageous steps from regions where singular points are repelling. This can be seen by considering the fitness gradient S and the tangent vector v along a trade-off curve. One can conclude that directional evolution ceases at the singular strategy $(x^*, \psi(x^*))$ where $S \cdot v = 0$. Evolution drives the phenotype in the direction of the tangent vector if $S \cdot v > 0$ and away as long as $S \cdot v < 0$.

Although analytical results of critical functions are generally not available, numerical solutions with various initial points can be easily obtained and plotted even in complex models (see Figure 1.5). A singular strategy is evolutionary attracting or convergence stable, if the trade-off function is more concave or less convex than the critical function at the point of tangency. In other words, the second derivative of the trade-off curve is smaller than the second derivative of the critical function. Thus, this geometric method enables visualizing the evolutionary outcomes after possible trade-off curves are superimposed.

1.2.2 Invasion Boundaries

A graphical method for analyzing the mutant's ability to invade in a resident population in a two dimensional trait space are **Invasion boundaries**, short

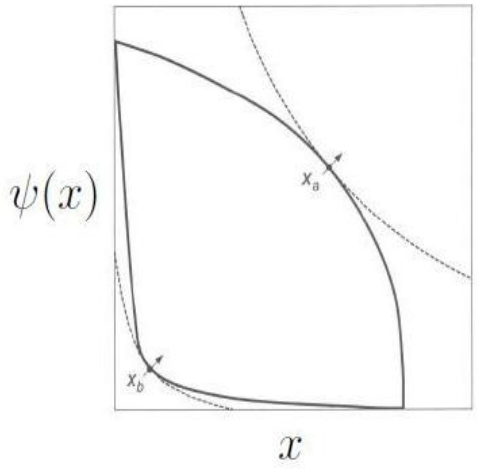

Figure 1.6: Thin dashed lines are I-boundaries. The solid lines are two trade-off curves, where x_a is a evolutionary stable strategy because the trade-off is concave and the I-boundary is convex. In the opposite case, x_b is not an ESS, since the trade-off curve is more convex then the I-boundary (Figure from De Mazancourt and Dieckmann (2004)).

I-boundaries (De Mazancourt and Dieckmann, 2004; Rueffler et al., 2004). For every resident population the trait space can be divided into a region of successful mutants ($\rho(x', x) > 0$) and unsuccessful mutants ($\rho(x', x) < 0$), respectively. The I-boundary to a corresponding resident strategy is a curve that separates these two regions. It is the line implicitly defined by $\rho(x', I(x'), x, \psi(x)) = 0$ that is tangent to trade-off curve at the singular strategy. For convex trade-offs singular strategies are locally uninvadible if the invasion boundaries is more convex than the trade-off curve at the point of tangency. For concave trade-offs singular strategies are locally uninvadible if the invasion boundaries are less concave than the trade-off curve at the point of tangency (see Figure 1.6).

Summing up, a population located at $(x^*, \psi(x^*))$ residing on the trade-off curve is evolutionary singular if the slope of the trade-off curve equals the slope of the I-boundary and the slope of the critical function at $(x^*, \psi(x^*))$. It is convergence stable if the curvature of the trade-off curve is smaller than the curvature of the critical function at $(x^*, \psi(x^*))$. It is evolutionary stable if the curvature of the trade-off curve is smaller than the curvature of the I-boundary at $(x^*, \psi(x^*))$. I denote the curvature of the trade-off curve at the singular strategy by K_T, the curvature of the critical function or A-boundary by K_A and the curvature of the I-boundary by K_I. The geometrical classification of singular points leads to the following conditions: A singular strategy $(x^*, \psi(x^*))$ is

1. a CSS whenever $K_T < K_A$ and $K_T < K_I$,
2. a branching point if $K_I < K_T < K_A$ and $K_A > K_I$,
3. a repellor if $K_I < K_T$ and $K_A < K_T$ and
4. a Garden of Eden point if $K_A < K_T < K_I$.

Chapter 2

The Model

I consider an ecological model in which a consumer is feeding on two resources that are assumed to be homogeneously distributed in space. The consumer is characterized by two quantitative evolving traits, that describe the relevant features of two modules both contributing to resource consumption. From this model I will derive the invasion fitness of mutant consumers and study the evolutionary dynamics to investigate the factors that favor division of labor among the modules and analyze if evolutionary branching can occur.

2.1 Ecological Model

Consider a consumer organism that feeds on two resources. The population dynamics is given by:

$$\begin{aligned} \dot{R}_1 &= r_1 - CF^1R_1 - d_1R_1 \\ \dot{R}_2 &= r_2 - CF^2R_2 - d_2R_2 \\ \dot{C} &= C(c_1F^1R_1 + c_2F^2R_2 - g) \end{aligned} \tag{2.1}$$

R_i denotes the population density of resource i ($i = 1, 2$) and C denotes the population density of the consumer. The growth rates r_1 and r_2 of the resources are independent of resource density and the resources grow constantly. The death rates of the resources are d_1 and d_2, respectively. So the population dynamics of the resources in absence of the consumers is described by chemostat dynamics. The consumer C has a constant death rate g. The parameters c_1 and c_2 are the conversion efficiencies of ingested resources into new consumers. The functions F^1 and F^2 denote the ability to consume resource 1 and 2, respectively. All parameters are summarized in Table 2.1.

System 2.1 has five equilibria. Four out of these five are not interesting since in all these equilibria at least one population is extinct. Setting the

Table 2.1: Notation
Note: All variables are positive.

Symbol	Definition
c_1,c_2	conversion efficiency of resource 1 and 2 respectively
C	consumer density
d_1,d_2	constant death rate of resource 1 and resource 2 resp.
g	constant death rate of consumer
F^1,F^2	performance functions
r_1,r_2	constant growth rates of resource 1 respectively resource 2
R_1, R_2	resource densities
θ_i	evolving trait

right-hand sides of (2.1) to 0, one obtains the equilibrium $(\hat{R}_1, \hat{R}_2, \hat{C})$, where

$$\hat{R}_i = \frac{r_i}{d_i + \hat{C}F^i}$$

for $i \in \{1, 2\}$ and

$$\hat{C} = \frac{c_1 r_1 F^1 F^2 + c_2 r_2 F^1 F^2 - d_2 F^1 g - d_1 F^2 g}{2gF^1F^2} + \frac{\sqrt{-4c_2 F^1 F^2 (d_2 F^1 - d_1 F^2) r_2 g + (F^1(F^2(c_1 r_1 + c_2 r_2) + d_2 g) - d_1 F^2 g)^2}}{2gF^1F^2}$$

The hat indicates equilibrium values. It is strictly positive if

$$c_1 r_1 d_2 F^1 + c_2 r_2 d_1 F^2 > d_1 d_2 g. \tag{2.2}$$

By the Routh-Hurwitz criterion (Hofbauer and Sigmund, 1998), if (2.2) holds and $r_1 = r_2$, $d_1 = d_2$, $c_1 = c_2$, then the ecological equilibrium is stable.

2.2 Performance Functions

The model applies to a consumer individual characterized by its two iterated modules. These modules both contribute to the same two biological functions, namely resource consumption. The modules determine the performance and adaptation for the two resources and therefore the consumption of them. They are described by quantitative traits θ_i, scaled such that $\theta_i \in [0, 1]$ for $i \in \{1, 2\}$. One can interpret the graphs of the scalar-valued performance functions $F^1(\theta_1, \theta_2)$ and $F^2(\theta_1, \theta_2)$ as performance landscapes

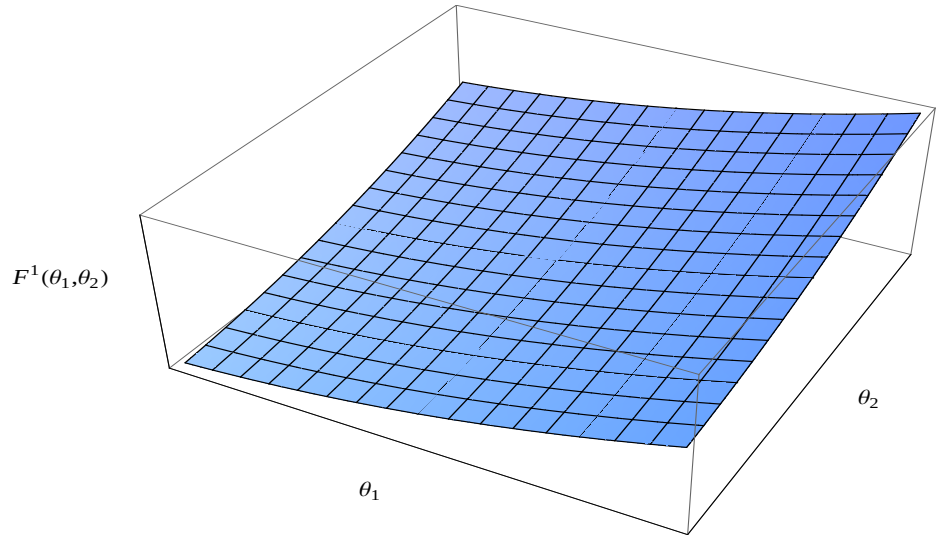

Figure 2.1: Three-dimensional plot of the convex increasing performance landscape F^1.

(see Figure 2.1). For example modules can be specialized limbs. For one resource such as mussels it is favorable for the consumer to have big claws but for plankton it is beneficial to have appendices that filter the nutrients out of the water.

Trade-offs in resource consumption exist nearly inevitably in nature. Improvements in certain traits and specialization for one resource in return, leads to poor adaptations for other resources. I follow Rueffler and Wagner (in rev.) and assume that there exists a trade-off in consuming resources in this model. To incorporate the trade-off I assume without loss of generality, that F^1 is increasing (see Figure 2.1) in both arguments and F^2 is decreasing in both arguments, i.e.:

$$\frac{\partial F^1(\theta_1,\theta_2)}{\partial \theta_i} > 0 \tag{2.3}$$

and

$$\frac{\partial F^2(\theta_1,\theta_2)}{\partial \theta_i} < 0 \tag{2.4}$$

for $i \in \{1,2\}$.
Specifically, if the trait values are equal to one ($\theta_1, \theta_2 = 1$), then the consumer is specialized for resource 1 and has its maximum performance but is poorly adapted to resource 2. Specialists with maximal performance for resource 2 are characterized by trait values equal to zero ($\theta_1, \theta_2 = 0$).

In my work I will describe the performance functions by second order Taylor polynomials:

$$F^1(\theta_1,\theta_2) = \alpha_1 + \beta_{11}(\theta_1-\theta_s) + \beta_{12}(\theta_2-\theta_s) + \frac{1}{2}(\gamma_{11}(\theta_1-\theta_s)^2 + \gamma_{12}(\theta_2-\theta_s)^2 + 2\delta_1(\theta_1-\theta_s)(\theta_2-\theta_s)) \quad (2.5)$$

$$F^2(\theta_1,\theta_2) = \alpha_2 + \beta_{21}(\theta_1-\theta_s) + \beta_{22}(\theta_2-\theta_s) + \frac{1}{2}(\gamma_{21}(\theta_1-\theta_s)^2 + \gamma_{22}(\theta_2-\theta_s)^2 + 2\delta_2(\theta_1-\theta_s)(\theta_2-\theta_s)) \quad (2.6)$$

The parameters γ_{ij} for $i \in \{1,2\}$ describe the curvature of the performance functions F^1 and F^2 in the direction of the axes of the trait space. If γ_1 and γ_2 are positive, F^1 and F^2 are convex curves, whereas for negative γ_1 and γ_2 the performance curves are concave.

The parameters δ_{ij} for $i \in \{1,2\}$ represent interactions between the modules. They describe how a change in one trait is affected by a change in performance due to a change on the other trait. The effect can be either amplifying or diminishing for the performance. Positive interacting modules mutually enhance each other and the performance value increases, while negative interaction reduces the value of performance for a resource. It will become apparent, that those factors mainly determine the evolutionary dynamics.

In these formulas $\theta_s \in [0,1]$ is a parameter. From now on I use the shortcut $\Big|_*$ for $\Big|_{\theta_1=\theta_2=\theta^*}$. The coefficients of the performance functions are:

$$F^i(\theta_s,\theta_s) = \alpha_i$$

$$\frac{\partial F^i(\theta_1,\theta_2)}{\partial \theta_j}\Big|_s = \beta_{ij}$$

$$\frac{\partial^2 F^i(\theta_1,\theta_2)}{\partial {\theta_j}^2}\Big|_s = \gamma_{ij}$$

$$\frac{\partial^2 F^i(\theta_1,\theta_2)}{\partial \theta_1 \partial \theta_2}\Big|_s = \delta_i$$

for $i,j \in \{1,2\}$. Only combinations of $\theta_s, \alpha, \beta, \gamma, \delta$ are considered where performance stays positive.

Substitutable Modules

Following Rueffler and Wagner (in rev.) I call two modules with respect to the i-th task substitutable if the function $F^i(\theta_1, \theta_2)$ is symmetric, i.e., if

$$F^i(\theta_1, \theta_2) = F^i(\theta_2, \theta_1) \tag{2.7}$$

for all $\theta_1, \theta_2 \in [0, 1]$.

If

$$\begin{aligned}\beta_1 &:= \beta_{11} = \beta_{12}\\ \beta_2 &:= \beta_{21} = \beta_{22}\\ \gamma_1 &:= \gamma_{11} = \gamma_{12}\\ \gamma_2 &:= \gamma_{21} = \gamma_{22}\end{aligned}$$

then it follows that modules are substitutable.

As a starting point I assume that the performance functions are symmetric in the sense that:

$$\begin{aligned}\alpha &:= \alpha_1 = \alpha_2\\ \beta &:= \beta_1 = -\beta_2\\ \gamma &:= \gamma_1 = \gamma_2\\ \delta &:= \delta_1 = \delta_2\end{aligned}$$

Note that the sign of β_2 is negative because I assumed that the performance function F^2 is decreasing.

Non-substitutable Modules

If two modules are non-substitutable with respect to at least one of the biological functions, then the modules are contributing differently to each task. Examples, already discussed in Chapter 1, are modules such as teeth or limbs. The position of a module in an organism can lead to different contributions for executing different tasks, e.g., anterior teeth are more efficient to contribute in cutting than posterior ones. Following Rueffler and Wagner (in rev.) I refer to this as positional effects. In the non-substitutable case the performance functions F^1 and F^2 are as in Eq. 2.5 and Eq. 2.6.

2.3 Evolutionary Dynamics

To derive the fitness function for the invading mutant in the population model one has to consider a mutant consumer with a slightly different trait

θ'. The dynamic of the System 2.1 extended by a mutant is given by:

$$\begin{aligned}
\dot{R}_1 &= r_1 - CF^1R_1 - C'F^1R_1 - d_1R_1 \\
\dot{R}_2 &= r_2 - CF^2R_2 - C'F^2R_2 - d_2R_2 \\
\dot{C} &= C(c_1F^1R_1 + c_2F^2R_2 - g) \\
\dot{C'} &= C'(c_1F^1R_1 + c_2F^2R_2 - g)
\end{aligned} \tag{2.8}$$

where C' denotes the population density of mutant consumers.

The initial growth rate of a rare mutant population (or invasion fitness function) in an environment where the resource abundance is determined by the resident population is given by:

$$\rho(\theta_1', \theta_2', \theta_1, \theta_2) = c_1F^1(\theta_1', \theta_2')\hat{R}_1(\theta_1, \theta_2) + c_2F^2(\theta_1', \theta_2')\hat{R}_2(\theta_1, \theta_2) - g \tag{2.9}$$

Keep in mind that the invasion fitness function includes the information of the environmental equilibria. In my model the mutant and resident are only interacting in an indirect way via competition for the same resources.

Chapter 3

Analytical & Numerical Results

In this chapter I will present the analytical and numerical results. In section 3.1 I analyze the scenario where the modules are scalars. I determine the singular points to analyze their invadibility and then their convergence stability. In section 3.2 I analyze singular strategies in the two dimensional space, where the two modules can be different.

3.1 Constrained Evolution

I assume that evolving consumers have ancestrally undifferentiated modules and consider the scenario where the two iterated modules have identical characteristics:

$$\theta_1 = \theta_2 = \theta.$$

Consequently, the phenotype can be described by a scalar θ in the one dimensional trait space. I refer to this one-dimensional trait space as **constrained trait space**. The values of the constrained space are located on the main diagonal in Figure 3.8. To find singular points θ^* the first derivative of the fitness function (2.9) is set to zero:

$$c_1 \frac{\partial F^1(\theta', \theta')}{\partial \theta'}\Big|_* \hat{R}_1(\theta^*, \theta^*) + c_2 \frac{\partial F^2(\theta', \theta')}{\partial \theta'}\Big|_* \hat{R}_2(\theta^*, \theta^*) = 0. \tag{3.1}$$

Analytically it is not possible to find all the singular point and it is also impossible to tell how many singular points exist. For symmetric performance parameters one singular strategy is located at $\theta^* = \theta_s$. For further symmetry assumptions, where the growth and death rates of the resources are equal and where the performance functions are symmetric around $\theta_s = 0.5$, one singular point is located at $\theta^* = 0.5$ (see Figure 3.1(a)). If the model is symmetric, the 'generalist' strategy is always an evolutionary singular

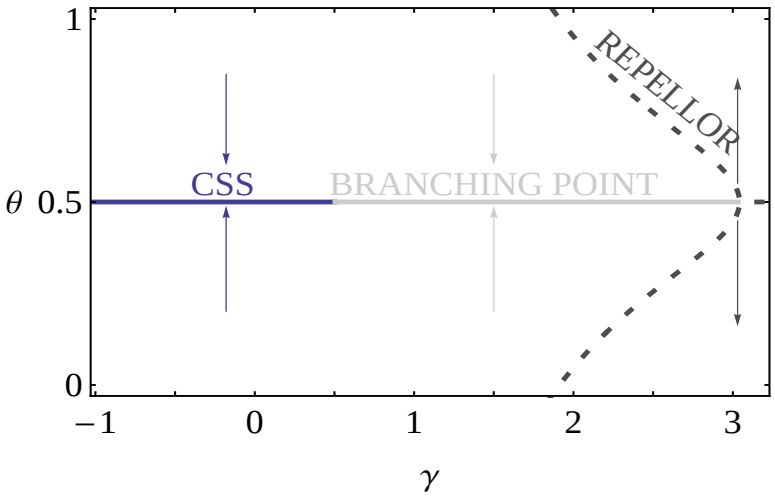

Figure 3.1: Bifurcation diagram of evolutionary singularities as a function of parameter γ of the performance landscape for $\delta = -0.5$ in the 45°-direction. The blue line indicates that the singular point is convergence stable, the gray line that it is a branching point and the dashed line that the singular point is a repellor. Arrows indicate the direction of evolutionary change. The figure shows the evolutionary properties of the singularities on the main diagonal. The regions of the three different evolutionary scenarios are shifted to the left with increasing δ and to the right by decreasing δ. Parameter values are $\alpha = 7/16$, $\beta = 3/4$, $r = 1$, $g = 0.1$, $c = 1$, $d = 0.1$ and $\theta_s = 0.5$.

strategy. Figure 3.1(a) shows that there exist two more singular strategies for certain parameter values of α, β, γ and δ. Since these other strategies are repelling I will not analyze them separately. In more realistic scenarios where resources are asymmetric the singular point is no longer at 0.5 but shifts along the main diagonal. It gets bigger than 0.5, if increasing the growth rate $r_1 > r_2$ or decreasing the death rate $d_1 < d_2$ of resource 1. It is shifted downwards the main diagonal if $r_1 < r_2$ or $d_1 > d_2$ which means that resources 2 is more abundant. The singular point shifts as well along the main diagonal following the same pattern whenever the performance functions are not fully symmetric. The bifurcation diagram for asymmetric resources is represented in Figure 3.4.

Evolutionary Stability

Whether singular points are evolutionary stable or evolutionary unstable can be seen by considering the second derivative of the fitness function evaluated

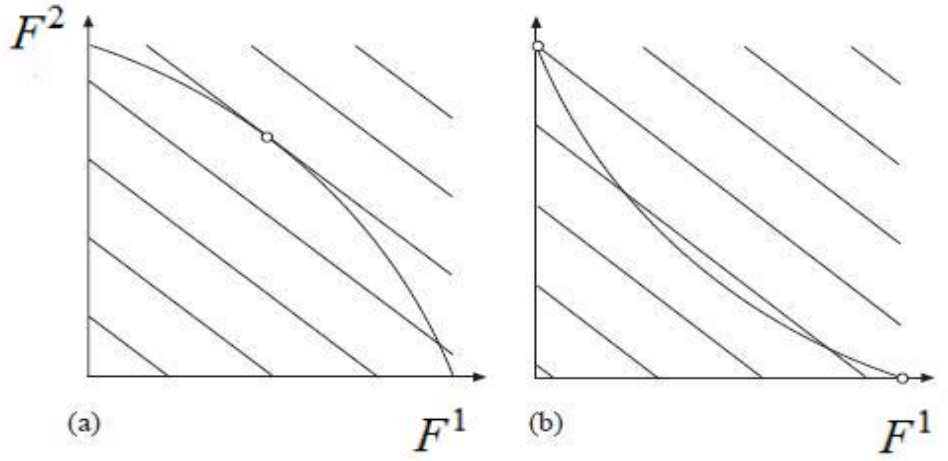

Figure 3.2: Trade-off curves for different values of the curvature parameters. The parameter of the performance functions determine the shape of the trade-off curve. If $\delta = 0$ and $\gamma = 0$ the trade-off is linear; (a) for $\gamma > 0$ it is concave; (b) for $\gamma < 0$ it is convex. The circles refer to these points with highest fitness.

at the singular point:

$$\frac{\partial^2 \rho(\theta', \theta', \theta, \theta)}{\partial \theta'^2}\Big|_* = [c_1 \frac{\partial^2 F^1(\theta', \theta')}{\partial \theta'^2} \hat{R}_1(\theta, \theta) + c_2 \frac{\partial^2 F^2(\theta', \theta')}{\partial \theta'^2} \hat{R}_2(\theta, \theta)]\Big|_* . \quad (3.2)$$

For the symmetric model $\frac{\partial^2 F^1(\theta', \theta')}{\partial \theta'^2}\Big|_* = \frac{\partial^2 F^2(\theta', \theta')}{\partial \theta'^2}\Big|_* = \gamma + \delta$. Furthermore $\hat{R}_1(\theta^*, \theta^*) = \hat{R}_2(\theta^*, \theta^*)$ holds. Therefore, the parameters γ and δ determine the sign of Eq. 3.2.

- The singular point is a fitness minimum (or expression (3.2) is positive) if and only if

  $$\gamma > -\delta.$$

  The point is invadible.

- The singular point is a fitness maximum (ESS), if and only if

  $$\gamma < -\delta.$$

  The point is uninvadible.

One can analyze invadibility of singular points geometrically too. To perform this geometrical analysis one expresses performance in the second

task as a function of performance of the first task $F^2 = \psi(F^1)$. For the symmetric model the trade-off function is as follows:

$$\psi(F^1) = \frac{4\beta^2 - 4\beta\sqrt{\beta^2 + (F^1 - \alpha)(\gamma + \delta)} + F^1(\gamma + \delta)}{(\gamma + \delta)} \tag{3.3}$$

The function ψ describes a trade-off curve parameterized with F^1 in the (F^1, F^2)-plane to which evolutionary change is restricted. By plotting a trade-off curve one can visualize the relation between performance function F^1 and performance function F^2. Since the invasion boundaries are linear in the two performance functions one can conclude that the sign of the curvature of the trade-off curve determines the invadibility of the singular point. Therefore it follows:

A singular point is uninvadible if and only if the trade-off curve is convex in the same direction of trait space ($\frac{\partial^2 \psi(F^1)}{\partial {F1}^2} > 0$).

A singular point is invadible if and only if the trade-off curve is concave in the same direction of trait space ($\frac{\partial^2 \psi(F^1)}{\partial {F1}^2} < 0$).

In the symmetric case the two parameters γ and δ determine the shape of the trade-off curve. Under a weak (concave) trade-off ($\gamma < -\delta$) the generalist strategy equally adapted to both resources is uninvadible for mutants (see Figure 3.2(a)). If the parameter $\gamma > -\delta$ (strong trade-off), the trade-off curve is convex. In this case such singular points are invadible (see Figure 3.2(b)).

When modules are non-substitutable, the singular point is not located on the main diagonal anymore. It is analytically not possible to tell where the singular strategy is located but numerical determination is possible. Nevertheless one can give a condition for uninvadibility and convex trade-offs in the constrained space:

$$-\frac{\beta_{21} + \beta_{22}}{\beta_{11} + \beta_{12}}(\gamma_{11} + \gamma_{12} + 2\delta_1) < (\gamma_{21} + \gamma_{22} + 2\delta_2). \tag{3.4}$$

The simplified Condition 3.1 for the symmetric model, but also for the unsymmetric model can be derived from Condition 3.4. The simplified condition for the asymmetric model where consumers have substitutable modules can be found in the Appendix A.

Convergence Stability

A singular point is convergence stable if and only if

$$\begin{aligned}\Big[& c_1 \frac{\partial^2 F^1(\theta', \theta')}{\partial {\theta'}^2} \hat{R}_1(\theta, \theta) + c_2 \frac{\partial^2 F^2(\theta', \theta')}{\partial {\theta'}^2} \hat{R}_2(\theta, \theta) \\ & + c_1 \frac{\partial F^1(\theta', \theta')}{\partial \theta'} \frac{\partial \hat{R}^1(\theta, \theta)}{\partial \theta} + c_2 \frac{\partial F^2(\theta', \theta')}{\partial \theta'} \frac{\partial \hat{R}^2(\theta, \theta)}{\partial \theta} \Big]\Big|_* < 0\end{aligned} \tag{3.5}$$

For the symmetric case convergence stability is analytically determinable:

- The singular point is convergence stable (selection drives the nearby phenotypes towards the singular strategy) if and only if

$$\frac{\gamma+\delta}{\beta^2} < \frac{1}{\alpha}(2-\frac{dg}{cr\alpha}). \tag{3.6}$$

- The singular point is repelling if and only if

$$\frac{\gamma+\delta}{\beta^2} > \frac{1}{\alpha}(2-\frac{dg}{cr\alpha}). \tag{3.7}$$

One can conclude that an evolutionary stable singular strategy is more likely to be convergence stable since in this case $\gamma+\delta$ are negative.

For the symmetric case one can show that only three out of four evolutionary scenarios are possible for the singular point as long as $F^1+F^2 \geq 2\alpha$. Then singular strategies can only be CSSs, BPs or repellors. If the performance functions are not big enough a Garden of Eden point gives a contradiction to the latter inequality and the population would go extinct.

In the asymmetric case it is not possible to derive convergence stability of singular points analytically. However, convergence stability can be analyzed geometrically. Numerical conditions for asymmetric resources and asymmetric performance functions are not shown here, but Critical Function Analysis is done instead. Once one has given a trade-off function, one can quickly and visually identify evolutionarily singular points and their convergence stability via this method.

The slope at a strategy $(F^1, \psi(F^1))$ is derived by solving equation (3.1) and rewriting it gives the following ordinary differential equation:

$$\frac{\partial \psi_{cr}}{\partial F^1} = -\frac{\hat{R}_1(F^1)}{\hat{R}_2(F^1)} \tag{3.8}$$

For symmetric resources equation (3.8) can be rewritten in the form

$$\psi\prime_{cr}(F^1) = \frac{-d(F^1-\psi_{cr}(F^1))g}{2c(F^1)^2 r} - \frac{\sqrt{4c^2(F^1)^2(\psi_{cr}(F^1))^2r^2 + d^2(F^1)^2g^2 - 2d^2F^1\psi_{cr}(F^1)g^2 + d^2(\psi_{cr}(F^1))^2g^2}}{2c(F^1)^2 r} \tag{3.9}$$

The family of critical functions are solutions of Equation (3.9), each belonging to a different initial condition (see Figure 3.3, for symmetric resources). Although solutions of this ordinary differential equation cannot be derived analytically, numerical solutions are easily obtained. Note, that for symmetric resources the critical functions are symmetric.

The ordinary differential equation for asymmetric resources is not presented. In the symmetric model critical functions are always convex. If

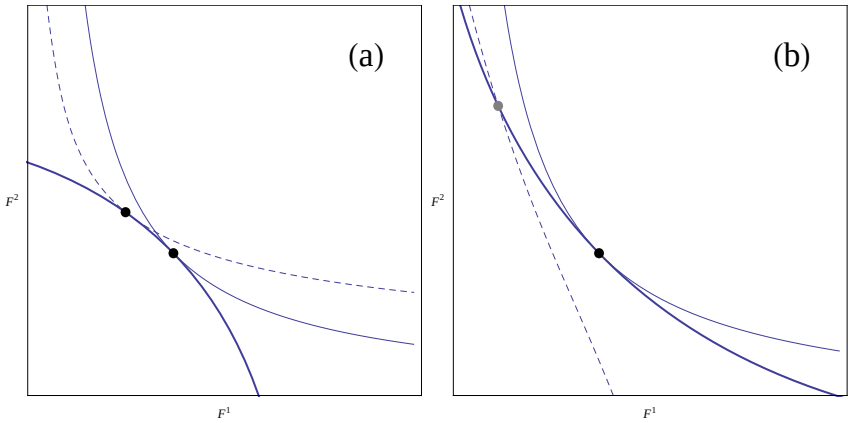

Figure 3.3: Panel (a) shows critical functions and the concave trade-off curve (solid curve). The thin curve denotes the critical function $\psi_{cr}(F^1)$ as obtained from numerical integration of Eq.(3.9) when resources are symmetric and the singular point is $\theta^* = 0.5$. The dashed curve denotes the critical function $\psi_{cr}(F^1)$ as obtained from numerical integration when the resources are asymmetric and the change of the singular point at $\theta^* = 0.3$. The black point means that the singular point is convergence stable whereas the gray point is not convergence stable. In panel (b) the trade-off function is convex and the singular point in the symmetric case shifts from $\theta^* = 0.5$ to $\theta^* = 0.24$ where resources become asymmetric. The singular point for asymmetric resources is not convergence stable anymore. Parameter values are as follows: Panel (a): $c_1 = c_2 = 1, d_1 = d_2 = 0.1, g = 0.1, r_1 = 1, r_2 = 2.5, \delta = -0.5, \gamma = -1$, Panel (b): $c_1 = 1, c_2 = 1.5, d_1 = 2, d_2 = 3.5, g = 1, r_1 = 4, r_2 = 3, \delta = 0, \gamma = 1$ (if parameter not mentioned see Figure 3.1).

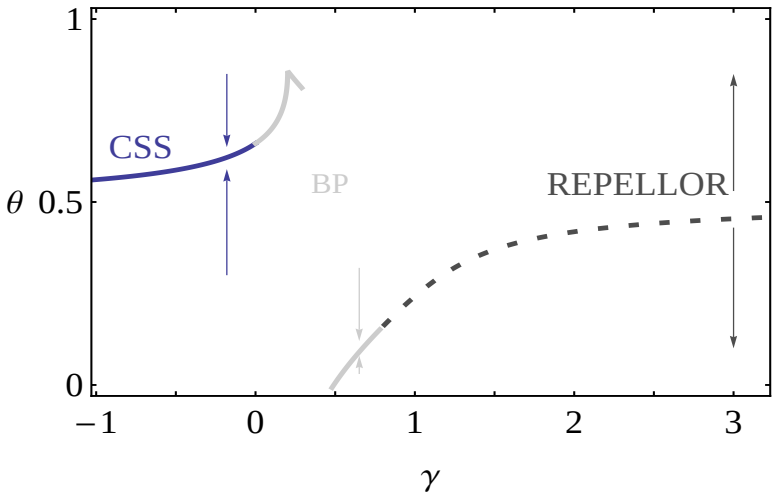

Figure 3.4: Bifurcation Diagram for asymmetric resources. Parameter values are as in Figure 3.3 Panel (*b*).

$r_1 \neq r_2$ critical functions stay convex. Using (3.8) gives the following condition:

$$\psi''_{cr}(F^{1*}) < \frac{\hat{R}_1(F^{1*})\hat{R}_2{}'(F^{1*}) - \hat{R}_2(F^{1*})\hat{R}_1{}'(F^{1*})}{(\hat{R}_2(F^{1*}))^2} \tag{3.10}$$

where $\hat{R}_i{}'(F^{1*})$ denotes $\frac{\partial \hat{R}_i(F^1)}{\partial F^1}\Big|_*$ and $F^{1*} = F^1(\theta^*, \theta^*)$. A trade-off function that is less convex or more concave at the singular point than the critical function is convergence stable. Numerical examples show that there is a decrease in the curvature of critical functions if resources are asymmetric. Singular points are shifted along the trade-off curve and can loose the property of convergence stability (see Figure 3.3). Figure 3.4 presents a bifurcation diagram for asymmetric resources. The singular strategies are not located at the center of trait space. The singular strategy $(\theta^*, \theta^*) = (0.24, 0.24)$ in panel (b) of Figure 3.3 is not convergence stable. This can also be read from the bifurcation diagram. The singular strategy is an evolutionary repellor.

In the case where modules are non-substitutable all numerical examples show that the family of critical functions are convex. Some numerical examples are shown in the Section 3.2.2 and in Chapter 4 simulations results of some examples are presented.

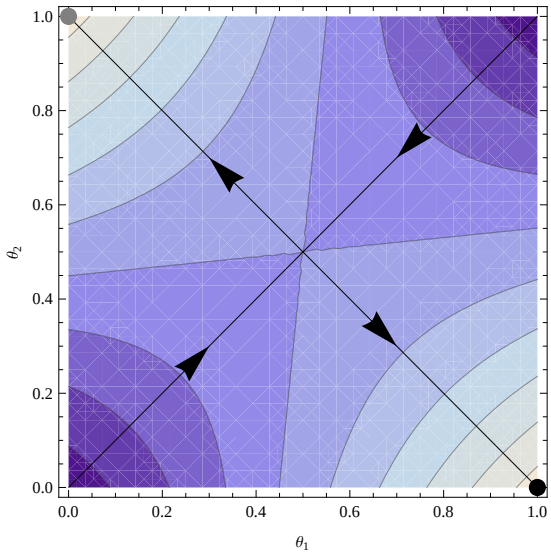

Figure 3.5: The trait value θ_1 is plotted on the x-axis and the trait value θ_2 is plotted on the y-axis. Individuals with undifferentiated trait values (located on the main diagonal of trait space) evolve to the singular point $(0.5, 0.5)$ where the two black lines are intersecting each other. At this point the individuals experience disruptive selection and evolve towards one of the two corners as indicated with the arrows. Phenotypes not lying on the main diagonal (where $\theta_1 \neq \theta_2$) have developed a pattern of division of labor.

3.2 Unconstrained Evolution

So far, I described the dynamics in the constrained space. Division of labor is the differentiation of modules contributing differently to the consumption of a resource. Individuals with a pattern of division of labor are not lying on the main diagonal (see Figure 3.5). Division of labor occurs in cases where the singular point is a CSS on the main diagonal and a repellor in the orthogonal direction. Division of labor can evolve if the singular strategy is a BP in the 45°-direction and repelling in the −45°-directions, depending on the shape of fitness landscape (evolutionary branching without division of labor is also possible). The evolutionary behavior of a singular strategy that is repelling in all directions is depending on the direction of the steepest increase in the fitness and the location of the population. In this case division of labor is a feasible scenario. To know what is happening locally around the singular point, a two-dimensional analysis is done in the next section.

3.2.1 Substitutable Modules

In this section I present the analysis of the unconstrained two-dimensional model starting at the singular point of the constrained space. The eigenvalues of the two-by-two Hessian matrix specifies the curvature of the fitness landscape at the singular point.

$$\mathsf{H} = \left(\begin{array}{cc} \frac{\partial^2 \rho(\theta_1', \theta_2', \theta_1, \theta_2)}{\partial {\theta_1'}^2} & \frac{\partial^2 \rho(\theta_1', \theta_2', \theta_1, \theta_2)}{\partial \theta_1' \partial \theta_2'} \\ \frac{\partial^2 \rho(\theta_1', \theta_2', \theta_1, \theta_2)}{\partial \theta_2' \partial \theta_1'} & \frac{\partial^2 \rho(\theta_1', \theta_2', \theta_1, \theta_2)}{\partial {\theta_2'}^2} \end{array} \right) \Big|_* \tag{3.11}$$

Since $h_{12} = h_{21}$, the Hessian matrix is symmetric. Under the assumption that modules are substitutable, the entries on the diagonal are also equal to each other ($h_{11} = h_{22}$).

Thus, the Hessian has the structure

$$\mathsf{H} = \begin{pmatrix} h_{11} & h_{12} \\ h_{12} & h_{11} \end{pmatrix}. \tag{3.12}$$

For such a matrix H, one can easily show that the eigenvectors are $(1, 1)$ and $(-1, 1)$. The eigenvalues are $\lambda_1 = h_{11} + h_{12}$ and $\lambda_2 = h_{11} - h_{12}$ to the eigenvectors $(1, 1)$ and $(-1, 1)$, respectively.

The sign of eigenvalue λ_1 determines the invadibility on the main diagonal. This condition is equal to the condition for invadibility in the constrained trait space (see page 23). The sign of the second eigenvalue determines the invadibility of the singular point in the orthogonal direction to the 45°-line. In the symmetric case $\lambda_2 = c(\gamma - \delta)(\hat{R}_1(\theta^*, \theta^*) + \hat{R}_2(\theta^*, \theta^*))$. Since the resource densities are always positive one can follow that:

- The eigenvalue λ_2 is positive if and only if

$$\gamma > \delta.$$

  Then the fitness landscape has a local minimum at θ^* and is invadable in the $-45°$-direction.

- The eigenvalue λ_2 is negative if and only if

$$\gamma < \delta,$$

  Then the invasion fitness has a local fitness maximum at θ^* and is uninvadable in the $-45°$-direction.

I derive the Jacobian matrix of the fitness gradient to determine the convergence stability of the singular point. The Jacobian is the sum of the Hessian H and the Q matrix.

$$\mathsf{J} = \begin{pmatrix} \frac{\partial^2\rho(\theta_1',\theta_2',\theta_1,\theta_2)}{\partial\theta_1'\partial\theta_1} + \frac{\partial^2\rho(\theta_1',\theta_2',\theta_1,\theta_2)}{\partial{\theta_1'}^2} & \frac{\partial^2\rho(\theta_1',\theta_2',\theta_1,\theta_2)}{\partial\theta_1'\partial\theta_2} + \frac{\partial^2\rho(\theta_1',\theta_2',\theta_1,\theta_2)}{\partial\theta_1'\partial\theta_2'} \\ \frac{\partial^2\rho(\theta_1',\theta_2',\theta_1,\theta_2)}{\partial\theta_2'\partial\theta_1} + \frac{\partial^2\rho(\theta_1',\theta_2',\theta_1,\theta_2)}{\partial\theta_2'\partial\theta_1'} & \frac{\partial^2\rho(\theta_1',\theta_2',\theta_1,\theta_2)}{\partial\theta_2'\partial\theta_2} + \frac{\partial^2\rho(\theta_1',\theta_2',\theta_1,\theta_2)}{\partial{\theta_2'}^2} \end{pmatrix}\Bigg|_* \tag{3.13}$$

As a result of the substitutability of the modules is $\frac{\partial F^1(\theta_1,\theta_2)}{\partial\theta_j}\Big|_* = \frac{\partial F^2(\theta_1,\theta_2)}{\partial\theta_i}\Big|_*$ and $\frac{\partial\hat{R}_1(\theta_1,\theta_2)}{\partial\theta_j}\Big|_* = \frac{\partial\hat{R}_2(\theta_1,\theta_2)}{\partial\theta_i}\Big|_*$ for $i \in \{1,2\}$. The entries of the Q matrix are all equal since the modules contribute equally to the performance functions. The derivative of the invasion fitness function with respect to θ_1 or θ_2 give the same entries. The simplified Jacobian is of the form

$$\mathsf{J} = \begin{pmatrix} q + h_{11} & q + h_{12} \\ q + h_{12} & q + h_{11} \end{pmatrix}$$

with eigenvalue $\lambda_1 = 2q + h_{11} + h_{12}$ to the eigenvector $(1,1)$ and $\lambda_2 = h_{11} - h_{12}$ to the eigenvector $(-1,1)$. Again, the condition for convergence stability along the main diagonal is the same as in the constrained case (see page 25). Note that the second eigenvalue from the Jacobian is equal to the second eigenvalue from the Hessian matrix. Therefore the invadibility and convergence stability properties in this direction are coupled and the sign of $h_{11} - h_{12}$ determines both uninvadibility and convergence stability in the $-45°$-direction.

Summing up, in the $-45°$-direction singular points are either CSSs or repellors.

- The singular point is a repellor if λ_2 is positive. This is the case if and only if

$$\gamma > \delta \tag{3.14}$$

  Then the fitness landscape has a local minimum at θ^* in the $-45°$-direction.

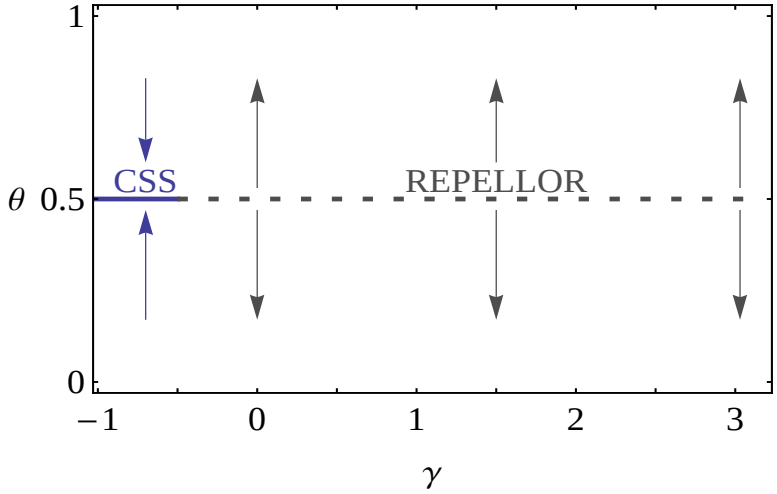

Figure 3.6: Bifurcation diagram of the evolutionary singular point as a function of parameter γ of the performance landscape for $\delta = -0.5$ in the $-45°$-direction. The figure shows the evolutionary properties of the singular point. The blue line indicates that the singular point is convergence stable and the dashed line that the singular strategy is a repellor. Arrows indicate the direction of evolutionary change. The regions of the two different evolutionary scenarios are shifted to the left (increasing δ results in a wider region for CSS points. By decreasing δ the region of repellors becomes bigger for even more convex performance functions. Parameter values are the same as in Figure 3.1.

- It is a CSS if λ_2 is negative. This is fulfilled if and only if

$$\gamma < \delta \tag{3.15}$$

  Then the fitness landscape has a local maximum at θ^* in the $-45°$-direction.

A Garden of Eden point or a branching point are not possible in the $-45°$-direction. It is intuitively clear that a branching point cannot emerge. Two individuals that are symmetric around a singular point on the $-45°$-line are selectively neutral. Their modules could be just numbered the other way round and then the two phenotypes are identical. But branching implies that two types on the opposite sides of the branching point can coexist and each of them has a selective advantage, when rare. Figure 3.6 presents the evolutionary properties of the singular point in the $-45°$-direction.

Along the $45°$-direction nothing changes compared to the unconstrained model (see the conditions on page 23 and page 25).

Table 3.1: Classification of Evolutionary Scenarios

		$-45°$	
		CSS	**REP**
$+45°$	**CSS**	Generalist	Divison of Labor
	BP	Polymorphism	Divison of Labor or Polymorphism
	REP	Single Specialist	Division of Labor or Single Specialist

Figure 3.7 shows the evolutionary outcome for the fully symmetric model. Uninvadibility depends on the two parameters γ and δ. Convergence stability in the 45°-direction is depending on all parameters of the performance function and on the ecological parameters, while the properties in the $-45°$-direction depends only on γ and δ. The blue line in Figure 3.7 separates the $(\gamma, \delta)-$ space into the region where a singular point is attracting or repelling, respectively in the 45°-direction. Under the black hatched line strategies are CSS in the 45°-direction and the black solid line is the borderline between continuously stable and repelling strategies in the $-45°$-direction. Hence, the (γ, δ)-plane can be divided into six regions where the singular strategy is

(1) a CSS on the main diagonal and a repellor on the second diagonal. In this region division of labor always evolves. Selection drives individuals with undifferentiated modules to the singular point. Once the population resides at the singular point it experiences selection away from the main diagonal towards one of the two corners in trait space where modules are functionally specialized and differentiated (see Figure 3.8(1)).

(2) a BP on the main diagonal and a repellor on the second diagonal. In this region both a polymorphic population and phenotypes with differentiated modules can evolve. Division of labor is not guaranteed and depends in which direction the fitness increases steeper at the singular point and, more importantly, on the availability of genetic variation. If $\delta > 0$ the polymorphic scenarios are favored more strongly and if $\delta < 0$ division of labor is favored more strongly. In Figure 3.8(2) represents the case where the population does not branch and individuals evolve as well into the regions of functional differentiation.

(3) a repellor on the main diagonal and a repellor on the second diagonal. The singular strategy in region (3) is repelling in all directions. Therefore, a monomophic population can evolve in any direction of the trait space. Figure 3.8(3) shows no points, but one can assume that a single specialist evolves since the fitness in the constrained direction has the steepest positive slope. Generally, one would not assume that the populations is located in the center of trait space. The closer the

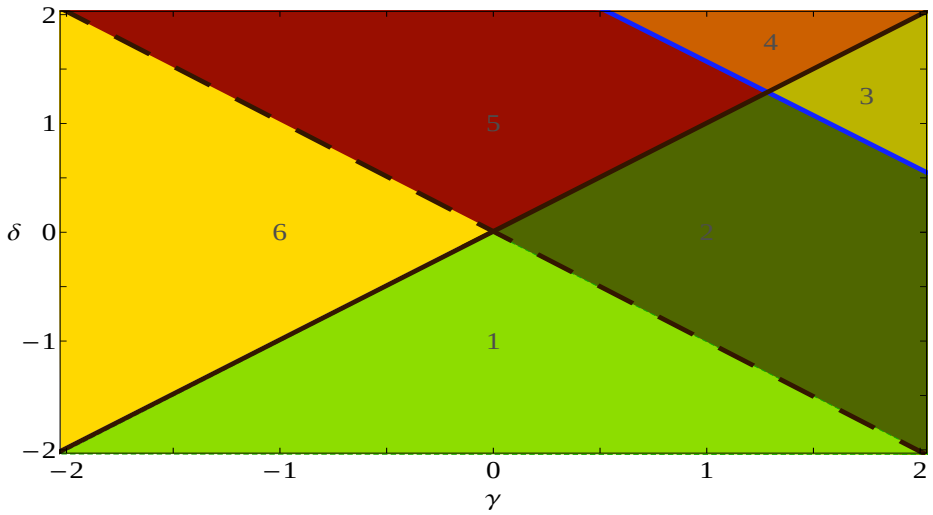

Figure 3.7: Evolutionary Dynamics at the singular point $\theta^* = 0.5$ with parameter values as in Figure 3.1. The x-axis is labels with the curvature parameter and the y-axis gives the interaction term γ. The under the blue line the singular strategy is convergence stable. The dashed black line is the borderline between invadibility and uninvadibility. The black line with positive slope gives separates the CSSs from the repellors in the $-45°$-direction of the trait space. The regions indicate (1) Division of labor, (2) Division of Labor/Polymorphism, (3) Division of Labor/ Single Specialist, (4) Single Specialist, (5) Polymorphism (6) Generalist (explanation in Table (3.1)). Parameter values are the same as in 3.1.

population is located to a corner the higher is the chance that it will evolve in this direction.

(4) a repellor on the main diagonal and a CSS on the second diagonal. The population will evolve to one of the corners with undifferentiated but specialized modules, with either $(\theta_1, \theta_2) = (0, 0)$ or $(1, 1)$. In this region (see Figure 3.8(4)) a single specialist evolves.

(5) a BP on the main diagonal and a CSS on the second diagonal. For parameter values in this region the population branches and becomes polymorphic. Two populations will evolve, each, with undifferentiated modules that are specialized for one of the resources (see Figure 3.8(5)).

(6) a CSS on the main diagonal and a CSS on the second diagonal. In this region the singular strategy is globally attracting and a fitness maximum, hence a CSS. All individuals evolve to become generalists. Selection drives all individuals to the center of trait space (Figure 3.8(6)).

The different evolutionary scenarios are summarized in Table 3.1.

If the two modules are substitutable with respect to both biological functions and the performance functions are not symmetric, then the condition

$$\frac{\frac{\partial F^2}{\partial \theta_2}\Big|_*}{\frac{\partial F^1}{\partial \theta_2}\Big|_*}(\gamma_1 - \delta_1) < (\gamma_2 - \delta_2) \tag{3.16}$$

indicates a saddle point. If the singular point is convergence stable in the 45°-direction. Functional differentiation is favored (see Rueffler and Wagner (in rev.)). Expression 3.16 means that each side is weighted by the rate of increase in performance in that trait.

The condition from the second eigenvector of the Jacobian $h_{11} - h_{12} > 0$ at the singular point (θ^*, θ^*) is equivalent (at the singular point) to

$$-\frac{\hat{R}_1}{\hat{R}_2}(\gamma_1 - \delta_1) < (\gamma_2 - \delta_2). \tag{3.17}$$

Then the singular point is a repellor in the $-45°$-direction and division of labor is favored in this direction. If the resource densities are equal at the singular point ($\hat{R}_1(\theta^*, \theta^*) = \hat{R}_2(\theta^*, \theta^*)$) or the parameter values of the performance functions are the same, then functional specialization and functional differentiation is favored if the sum of the interaction parameters is smaller than the sum of the curvature parameters (along the main axes) $(\delta_1 + \delta_2 < \gamma_1 + \gamma_2)$.

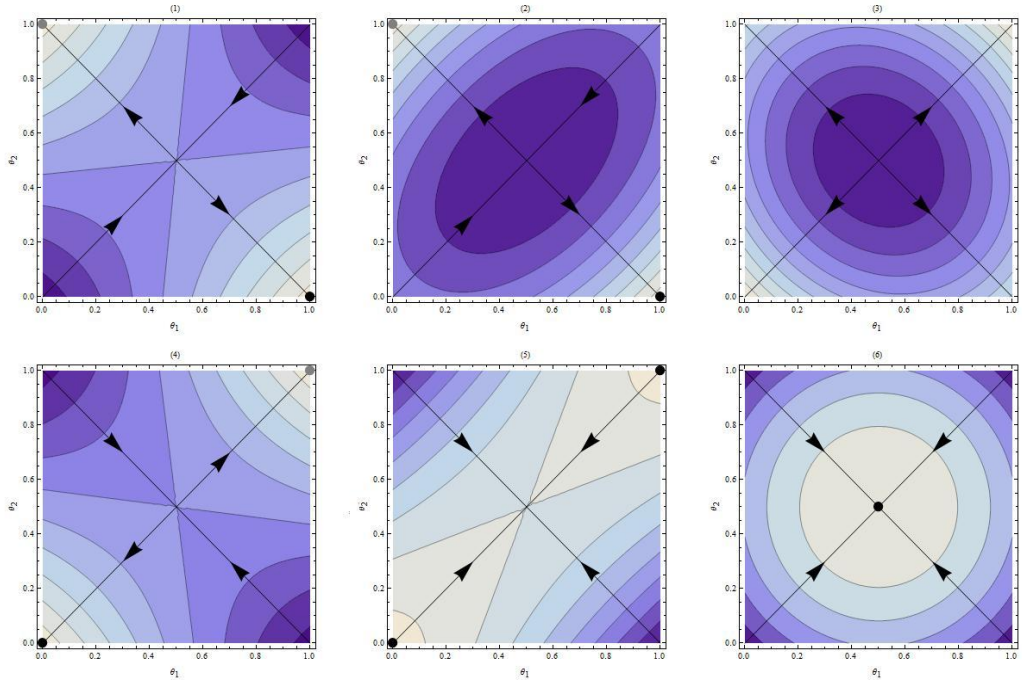

Figure 3.8: Evolutionary dynamics at the singular point $\theta^* = 0.5$. Gray scales correspond to contours of the fitness landscape where brighter zones indicate higher fitness values, given that the resident is at the singular point (as locally given by the Hessian). Arrows indicate the direction of the monomorphic ecological dynamics (as locally given by the Jacobian). If there are only black points in the figure the population is dimorphic . If there is a gray and a black point in the figure, then only one of the two populations are resident. Parameter values for each subfigure (regions are as in Figure 3.7): (1): $\delta = 2, \gamma = 0.4$,(2): $\delta = 2, \gamma = -1$,(3): $\delta = 0.5, \gamma = 3$,(4): $\delta = 4, \gamma = 1$,(5): $\delta = 1.5, \gamma = -1$,(6): $\delta = 0, \gamma = -2$ (other parameters as in Figure 3.1).

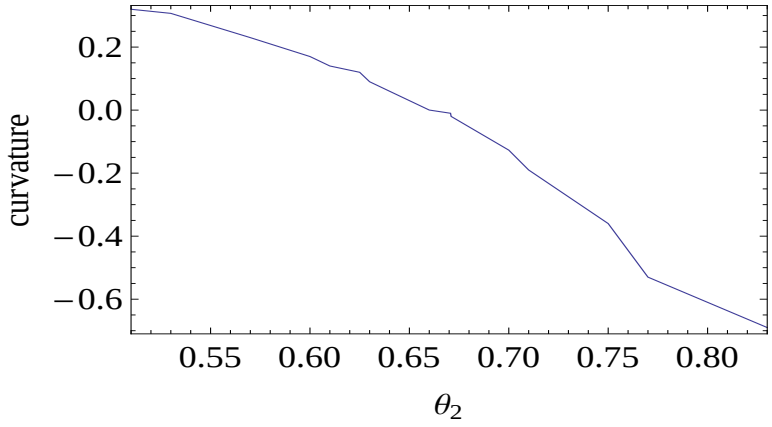

Figure 3.9: Decrease in the curvature of the fitness function in the 45°-direction by increasing the trait value θ_2 of the singular point $((1-\theta_2)^*, \theta_2^*)$. The singular point moves along the line in $-45°$-direction.

3.2.2 Non-substitutable modules

If the two modules are not substitutable the eigenvectors of the Jacobian and Hessian are generically not orthogonal at the singular point. In the presence of positional effects, functional specialization and differentiation is always favored. Due to the asymmetry introduced by non-substitutable modules, differentiation is only possible to one side from the main diagonal of the trait space. Since analytically no general conditions are found in the unconstrained space, numerical examples will be shown here. I want to investigate whether evolutionary branching arises once a pattern of division of labor has evolved. I start to analyze a singular strategy where the population has substitutable modules showing no pattern of division of labor. The singular strategy $(\theta_1^*, \theta_2^*) = (0.5, 0.5)$ is a branching point in the main diagonal and a CSS in the $-45°$-direction. Particularly, it is a fitness minimum along the main direction of trait space. Changing the parameters β_{ij} and γ_{ij} (for $i, j \in \{1, 2\}$), so that the modules get non-substitutable the singular point is located on the $-45°$-line of trait space. I change the parameter folling the pattern: $\beta_{11} = -\beta_{22} = -\gamma_{ii}$ and $\beta_{11} = 2\beta_{12} = -2\beta_{21} = -2\gamma_{ij}$. By increasing the parameter values and letting the others fixed, the singular strategy is shifted down along the line in $-45°$-direction. The curvature of the fitness function at the singular points along the 45°-direction decreases and the singular points become uninvadible. This example shows that the distance of the singular point to the center of trait space correlates with the shape of the curvature of the fitness function in the 45°-direction. It seems that division of labor decreases the possibility of polymorphisms (see Figure 3.9). I picked three examples and run simulations presented in Chapter 4.

Chapter 4

Simulation Results

The analytical results obtained so far are based on the Adaptive Dynamics approximation. In simulations one can see what scenarios arise if the assumptions from Adaptive Dynamics are relaxed and stochastic effects are implemented. More precisely, a finite population is fluctuating in size and trait distribution and is not at the equilibrium state. As a consequence there exist many mutant sub-populations at the same time. Mutation rates are assumed to be higher and therefore the assumption of the ecological and evolutionary time-scale separation is not fulfilled. The reason why individual-based simulations are important is to investigate the robustness of the results found with the Adaptive Dynamics method. Another reason for the simulations is to understand scenarios where the evolutionary dynamics is not analytically solvable. Therefore, I develop a program that simulates the more realistic dynamics. The program is written in Matlab and the Matlab source code '$ResourceCompetition\_1.m'$, is presented in Appendix B.0.3. All variables are listed in Table 4.1.

Section 4.1 contains the parts where I test the predictions of the analytical results and section 4.2 contains the parts where simulations helped to see what is happening where an analytical treatment is not possible.

4.1 Substitutable Modules

First, I investigate the completely symmetric model where the modules are substitutable and resources are assumed to be symmetric. In the following I present the results from simulations for the six different regions shown in Figure 3.7 which shows the evolutionary properties of the singular strategy at $\theta^* = 0.5$ as a function of the curvature parameter (along the main axes) γ and the interaction term δ. I start the simulations with an initial population unspecialized for any resource and showing no level of functional differentiation, located at the singular point, i.e., $\theta_1 = \theta_2 = 0.5$.

- In region (1) and (3)-(6) of Figure 3.7 the simulations confirm the

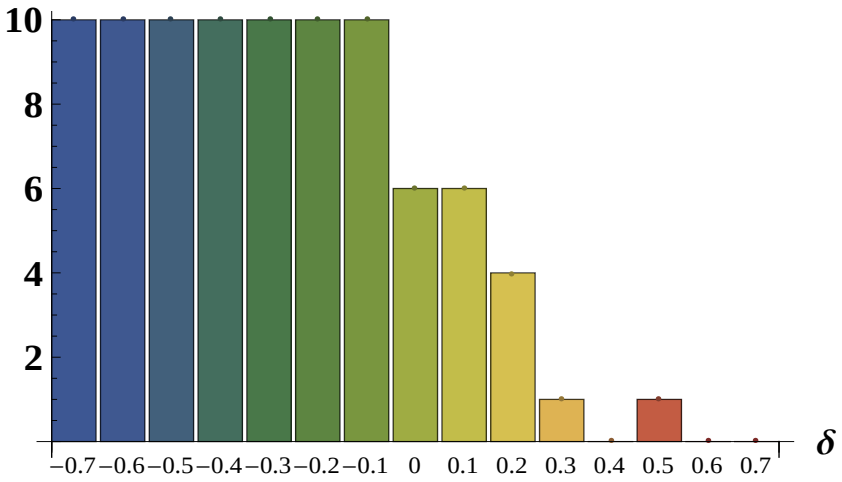

Figure 4.1: Frequency of evolutionary outcome of division of labor alternatively to polymorphisms (x-axis), dependening on the interaction parameter δ (y-axis). Ten runs are performed for different values of δ. For negative interaction values of δ, division of labor always evolves. The more positive the interaction parameter gets the more often evolutionary branching occurs, but division of labor stays possible. The simulation parameters: *pop* $= (0.5, 0.5, 1000)$, $\Delta = 0.01$, $\mu_1 = \mu_2 = 0.1$, $r_1 = r_2 = 100$, $\theta_s = 0.5$, $c_1 = c_2 = 1$, $d_1 = d_2 = 0.1$, $g = 0.1$, $\alpha_1 = \alpha_2 = 7/16$, $\beta = 0.75$, $\gamma = 0.75$.

Table 4.1: Input Values

Parameter	**Value**
pop	$(\theta_1, \theta_2, 1000)$
$tmax$	50000
μ_1	0.01
μ_2	0.01
Δ	0.01
$c_1 = c_2$	0.1
$d_1 = d_2$	0.1
g	0.01
$\alpha_1 = \alpha_2$	7/16
$\delta_1 = \delta_2$	1.5

predictions from the analytical analysis.

- Region (2) has to be considered in more detail, since analytical predictions are not clear. In this region both division of labor and polymorphisms are favored. I ran simulations along a transect at $\gamma = 0.75$ through parameter space to investigate if division of labor or polymorphisms evolve. Furthermore, I want to know if stochasticity plays a role for the evolutionary outcome. Therefore ten runs with 1000 individuals, located at the center of trait space, were performed. The simulations show that the number of individuals is unimportant for the evolutionary outcome. An increase in population size decelerates the speed of evolutionary change and increases the effort of the computational process. Mutation rates high (see the legend of Figure 4.1). Biologically more realistic mutation rates from 10^{-4} up to 10^{-5} are computationally too demanding. Figure 4.1 shows the frequency of how often division of labor, alternatively to polymorphisms evolved for different values of δ. For interaction parameter $\delta < 0$, in 100% of the runs division of labor evolved. Around the region with no interaction divison of labor still evolved but the frequency of this outcome decreases. Stochastic extinction might hamper evolutionary branching in regions where the interaction parameter δ is slightly positive. In cases with positive interaction division of labor still evolves but the evolutionary outcome of polymorphisms increases in frequency.

4.2 Non-substitutable modules

For populations with non-substitutable modules it is impossible to determine the exact evolutionary outcome analytically. In order to understand the evolutionary dynamics at the singular points that were found numerically in Section 3.2.2, simulations are performed. I investigate if polymorphisms

evolve once the population has functionally specialized and functionally differentiated modules. The input parameters are listed in Table 4.1. Parameters not mentioned in the Table varied in the simulations runs and are given in the legend of Figure 4.2. I pick three representing examples. For a population with substitutable modules the singular strategy resides at the main diagonal $(\theta_1^*, \theta_2^*) = (0.5, 0.5)$. The singular strategy is a evolutionary branching point. This remains valid in the simulations as shown in 4.2(g). Changing the parameters β_{ij} and γ_{ij} (for $i, j \in \{1, 2\}$) according to the pattern given in Section 3.2.2, the modules get non-substitutable. For example, one singular point is located at $(0.62, 0.38)$ on the $-45°$-line of trait space. This singular point is still an evolutionary branching point (see Panel (b) & (e)). Nevertheless, simulations do not confirm this evolutionary outcome. The population in this simulation stays around the singular strategy and does not branch (see Panel (h)). Again, I increase the parameters β_{ij} and γ_{ij}. The singular strategy located at $(0.7, 0.3)$ becomes a fitness maximum (see Panel (f)). As shown in Panel (c) of Figure 4.2 the singular strategy is a CSS in the $45°$-direction. In this scenario the simulations confirm the predicted evolutionary outcome (see Panel (i)). Once division of labor has evolved it seems that evolutionary branching in simulations is not possible.

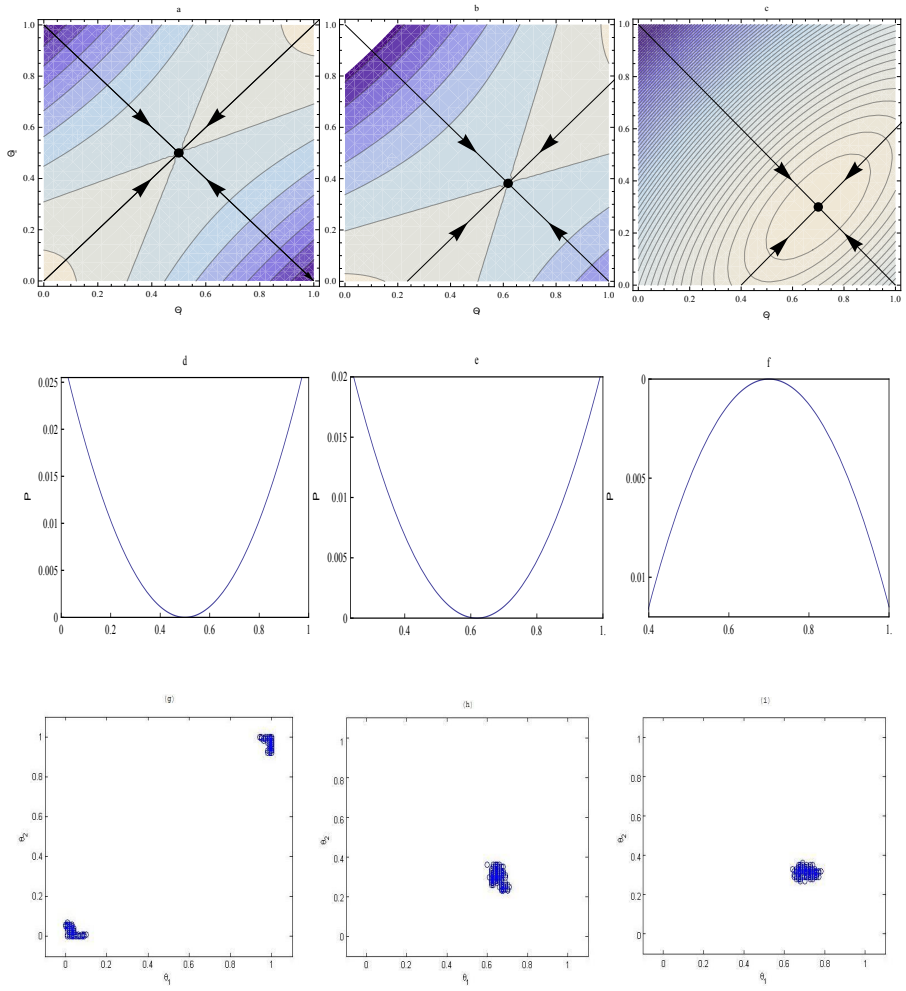

Figure 4.2: Panel $(a), (b)\&(c)$ represent the contour plots of the fitness landscape of the population residing at the singular point ((a): $(\theta_1^*, \theta_2^*) = (0.5, 0.5)$, (b):$(0.62, 0.38)$, (c):$(0.7, 0.3)$). Panel $(d), (e)\&(f)$ represents the fitness function around the singular point. Panel $(g), (h)\&(i)$ represents the simulation outcomes. In Panel (a) and (b) the singular points are BPs and in Panel (c) the singular point is a CSS in the 45°-direction. Introducing positional effects changes the evolutionary outcome. Numerically the singular point is a BP (Panel $(b), (e)$) but in the simulations the population does not branch (Panel (h)). The other simulations confirm the predicted outcome. Parameter values (if not listed see Figure 3.1 and Table 4.1): Panel (g): $\beta_{ij} = -\gamma_{ij} = 1$, Panel (h): $\beta_{ii} = -\gamma_{ii} = 3$, $\beta_{ij} = -\gamma_{ij} = 1.5$, Panel (i): $\beta_{ii} = -\gamma_{ii} = 1.1$, $\beta_{ij} = -\gamma_{ij} = 0.55$ for $i, j \in \{1, 2\}$.

Chapter 5

Conclusion & Discussion

In this work, with the methods of Adaptive Dynamics and Critical Function Analysis I analyze a predator-prey model. Predators forage on two types of prey. Foraging success of predators depends on the phenotype of two modules. These modules can for example be different pairs of appendages in crustaceans. In my study I investigate the evolutionary dynamics of the phenotype of such modules contributing to resource consumption. Several evolutionary outcomes are possible. First, consumers consist of two identical modules that are both equally adapted to both resources. Such consumers are resource generalists. Second, consumers consist of two identical specialized modules for one resource. Such consumers are resource specialists. Third, consumers consist of one module specialized for one resource and the other module specialized for the second resource. Such consumers consist of two modules that have evolved division of labor. In this model I consider frequency-dependent and density-dependent selection and investigate the situation where all three consumer populations can evolve. I assume that consumers' modules are ancestrally undifferentiated for any of the two resources and that specialization of the consumer's modules on one resource is assumed to go at the expense of specialization on the other resource. Thus, there exists at trade-off.

First, I analyze the symmetric model and assume that phenotypes of the two modules are constrained to be identical. Thus, I am investigating the evolutionary dynamics under the assumption that division of labor cannot evolve. Consumers evolve to become generalists when the trade-off curve is concave. Furthermore, generalist consumers are favored if modules interact negatively. In the case where the trade-off is slightly convex, the population evolves towards the generalist strategy, followed by evolutionary branching and the populations splits into two diverging subpopulations. For strong convex trade-offs and favored by positive interaction between modules consumers evolve to become single specialists. In the absence of interaction

between the modules, the findings match with the results found by Ma and Levin (2006), Rueffler et al. (2006b) and Zu et al. (2011). However, introducing interaction between modules helps to predict a trend of the evolutionary outcome.

In the second part of my analysis functional differentiation is allowed, which means that consumers are allowed to evolve division of labor. As already found by Rueffler and Wagner (in rev.) I show that the evolution of division of labor is favored when (*i*) convex trade-offs and (*ii*) negative interaction of the modules are present. By negative interactions I refer to interference between modules contributing to the same resource. In particular, the results of Rueffler and Wagner (in rev.) match with my results although their model is density- or frequency-independent. The matching exists because in both models contribution to resource consumption only depends on the phenotype of a consumer in question but not on the abundance and frequency of other phenotypes of the same species in the population. Furthermore, I show that in cases with slightly concave trade-offs and negative interaction between modules division of labor also evolves.

By using the method of Adaptive Dynamics assumptions are made that do not seem biological representative. Simulations allow more realistic scenarios, such as higher mutation probabilities and small populations sizes. Biologists may criticize that mutation rates are set too high, but if the results are robust for such high mutation rates, then they also hold for biological realistic mutation rates but just decelerate the speed of the evolutionary dynamics. I ran a number of individual-based-simulations to test the analytical results. In the symmetric model simulation runs confirm the analytical results. In some scenarios where trade-offs are slightly convex and interaction between modules is negative or slightly positive two evolutionary outcomes are possible: Evolutionary branching or division of labor. I find that with convex trade-offs and negative interaction division of labor is always favored and even for slightly positive interaction such outcomes are still possible. However, by increasing the interaction term even more, evolutionary branching is favored and the populations becomes dimorphic. It seems intuitively clear, that negative interaction forces the modules to specialize differently so that each module get specialized for one resource and division of labor evolves. Alternatively, if modules interact positively the emergence of division of labor can be prevented. Furthermore, evolutionary branching gets more likely when there is a strong selective constraint on division of labor. The development of division of labor is too costly in comparison to benefit immediately, when modules are interacting positively. As similarly noted in the work of Rueffler and Wagner (in rev.), I investigate another potential factor that explains the evolution of division of labor. Division of labor becomes inevitably by assuming that the consumer's mod-

ules contribute differently to resource consumption, for instance due to the position of the module within the organism. I follow Rueffler and Wagner (in rev.) and denote the third factor that favors functional differentiation as (*iii*) positional effects.

Van Dooren et al. (2004) studied a sex-specific phenotypic trait model of sexual dimorphisms versus evolutionary branching, looking at a broad range of ecological scenarios and investigated which phenotypic polymorphisms occur. They found that not only sexual selection but also ecological factors play a role to the widespread existence of sexual dimorphisms and claim that the possibility of evolutionary branching becomes unlikely when phenotypic differentiation between sexes and therefore sexual dimorphisms is allowed. These results match with the results I found by running more simulations. Evolutionary branching becomes more likely when there is a strong constraint on division of labor. In simulations where the evolution of division of labor is allowed to evolve and the population's modules contribute differently to resource consumption, branching does not seem to be very likely anymore. Even though some numerical results predict evolutionary diversification, I do not find scenarios where branching ocurrs and is maintained in the simulations after division of labor has evolved. In the model of Van Dooren et al. (2004) secondary branching events can occur after two sexual dimorphisms have evolved. This is not the case in my model. The population stays monomorphic once a population with functional differentiated modules has evolved. Branching only leads to two specialist populations. Leimar (2005) compared the possibility of evolutionary branching leading to genetic polymorphisms with the evolution of genetic monomorphic but phenotypically mixed strategies in different environments. His examples suggest that evolutionary branching is favored when spatial variation, together with less-than-random dispersal of individuals over habitats is assumed, whereas mixed strategies will evolve more likely if assuming large-scale temporal fluctuations and competition between relatives. In my model mixed strategies are equivalent to scenarios of division of labor. I expect that division of labor evolves in oscillating environments with for example seasonal changes, because the population would be more robust to changing or fluctuating environmental conditions. In compliance with these papers, it seems correct that evolutionary branching remains possible but becomes more unlikely division of labor is allowed.

Note, that I do not incorporate the possibility of mutational covariance between the traits in the simulations. This means that I do not allow for mutations that result in changes in both traits at the same time. Nevertheless, by incorporating mutational covariance between the two modules in the model I expect that evolution of division of labor gets hampered and that polymorphisms occur more frequently.

I expect that my results are robust to changes in the dynamics of the resources. For example, logistic growth for the resource instead of the chemostat dynamics or using different trade-offs should not affect qualitatively the evolutionary outcome (Ma and Levin, 2006; Zu et al., 2011).

Appendix A

Evolutionary Stability for asymmetric performance functions

For cases where performance functions are asymmetric ($\beta_1 \neq -\beta_2$, $\gamma_1 \neq \gamma_2$, $\delta_1 \neq \delta_2$) singular points are invaidible if and only if:

$$-\frac{\hat{R_1}}{\hat{R_2}}(\gamma_1 + \delta_1) < (\gamma_2 + \delta_2) \tag{A.1}$$

A singular strategy is uninvadible if the opposite holds. At the singular point $-\frac{\hat{R_1}}{\hat{R_2}} = -\frac{\beta_2}{\beta_1}$ holds. An equivalent condition to condition A.1 is therefore:

$$-\frac{\beta_2}{\beta_1}(\gamma_1 + \delta_1) < (\gamma_2 + \delta_2) \tag{A.2}$$

which matches with the condition of convex trade-off curves. So, if the trade-off curve is convex the singular point is invadible.

Appendix B

Programing

The program used for the simulations follows different phenotypes present in the population.

Figure B.1 gives a schematic representation of the program structure, and is explained in detail in the next section.

B.0.1 The Input Arguments

To run the program one has to determine the initial population structure, such as trait values and number of individuals, the model parameters and the parameters determining the mutational process (mutation rates μ_1, μ_2 and mutation step size Δ). The model parameters are the arguments of the performance functions and the parameters of the population dynamical system as in my model. The input arguments are summarized in Table B.1. The program consists of the following steps (see Figure B.1):

1. Determine the current resource densities as determined by the current population.

2. Determine the number of offspring by drawing form a Poisson distribution for each genotype in the population.

3. Determine the number of mutated individuals by drawing from a binomial distribution for each genotype.

4. Allocate the mutants to the different sub-populations and add the mutants with new trait combinations to the populations.

5. Update the genotype matrix by deleting the entries that are 0 (individuals that are extinct).

These steps are iterated until a maximal number of generations *tmax*. Note that there are stochastic effects in the simulations. By running the numerous simulations, one can see if the results are robust.

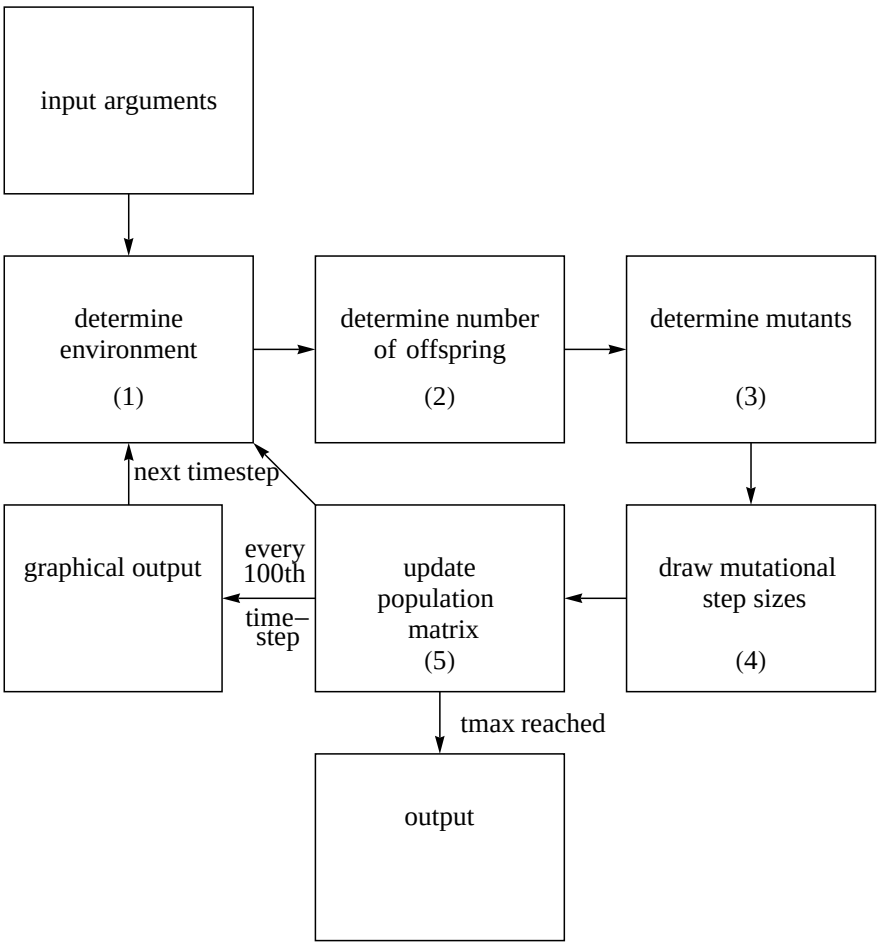

Figure B.1: Structure of the program

B.0.2 The Output

The output of the program includes a vector of length *tmax* with each entry giving the number of individuals in each generation (*nhist*), two vectors of the mean and the standard deviation of the two genotype values *theta1* and *theta2* respectively. Furthermore the program gives the genotype matrix (*pophist*). Each row of the genotype matrix contains the two trait values, the number of individuals carrying these trait combination and each 100th time step $(\theta_1, \theta_2, K, t)$ of the genotype matrix contains the trait values θ_1, θ_2 and the number K of individuals carrying this genotype and the time-step the population consisted of such variety.

Note that the case where mutations in both traits occur simultaneously is ignored. If there occurs a mutation in θ_1, then the individual will not mutate in the other trait θ_2. This does not mean, that it is biologically uncommon, but a mutation in the other trait is possible in the following generation. If you assume low mutation probabilities, the chance of double mutations becomes negligible.

The program was able to simulate the population dynamical system described in Chapter 2 with short running times and in an automatized way. It produces two different outputs: A graphical output (if not suppressed) as well as a numerical one. The graphical output can be observed while running the simulations. It can be used to qualitatively and directly track the trait values changing in the population. The numerical results keep a record of the population history. One can suppress the graphical output during the simulations but can still create graphical output from the saved data.

Graphical Output

Figure B.2 shows an example of different types of the graphical outputs produced by the program. Figure B.2 (a) shoes a phase diagram of the two trait variables θ_1 and θ_2. It shows the distribution of individuals in trait space. Each dot represents one individual. It displays information about the resident population. Because mutation step sizes are set low, it is clear that the trait values will not jump from one corner to the other. Conversely, the mutation rates are set high. There exists always a cloud of individuals with similar traits. A populations has branched if two discrete clusters appear in trait space.

Figure B.2 (b) shows the graph of the mean of θ_1 and θ_2 as a function of time. The trait values at time step 0 show that the simulation was started with a monomorphic population characterized by $(\theta_1, \theta_2, K) = (0.5, 0.5, 1000)$. This corresponds to the center of the phase diagram. The blue line in Figure B.2 (b) shows the mean of trait θ_1 whereas the red line

Table B.1: Input arguments

Name	Dimension	Definition
pop	n x 3	Genotype matrix of the initial population; each row containing (θ_1, θ_2, K) of one sub-population. n is the number subpopulation present in the population
tmax	scalar	number of generations the simulation runs
mPtheta1	scalar	mutation rate μ_1 of θ_1
mPtheta2	scalar	mutation rate μ_2 of θ_2
mS	scalar	mutation step Δ size
r	1x2	growth rates r_i for resource 1 and resource 2 resp.
d	1x2	death rates d_i for resource 1 and resource 2 resp.
c	1x2	conversion efficiency c_i for resource 1 and resource 2 resp.
g	scalar	death rate g of consumer
thetas	scalar	performance function parameter θ_s
alpha	1x2	performance function parameter α_i
beta	2x2	performance function parameter β_{ij}
gamma	2x2	curvature parameter of performance functions γ_{ij}
delta	1x2	interaction parameter of performance functions δ_i
noplot	scalar	suppresses graphical output if 1

shows for the mean of trait θ_2 over time. In this example the means of the two traits diverge, indicating a scenario where division of labor is evolves. The population evolves towards the corner $(\theta_1, \theta_2) = (1, 0)$ of trait space. Nevertheless, one has to look at Figure B.2(c) and B.2(d), which present the standard deviation of both traits as a function of time. The standard deviation of both trait values is close to 0. Only around generation 4000 there is an increase in the standard deviation which means that there is a certain amount of individuals carrying a higher or lower trait value θ_2 than the average. This can be also interpreted as noise. In previous generations the standard deviation is close to zero, which indicates that the population is not wide-spread.

B.0.3 Matlab Code

Here I present the commented Matlab source code of the program used for the simulations (see Svardal (2008)). Table B.1 explains the input arguments whereas Table B.2 the output variables. (Mathworks - Matlab $R2010a$7.10.0.499)

```
function[pophist,nhist,theta1mean,theta2mean,theta1std,theta2std]=...
ResourceCompetition_1(input)

%  function[pophist,nhist,theta1mean,theta2mean]=
```

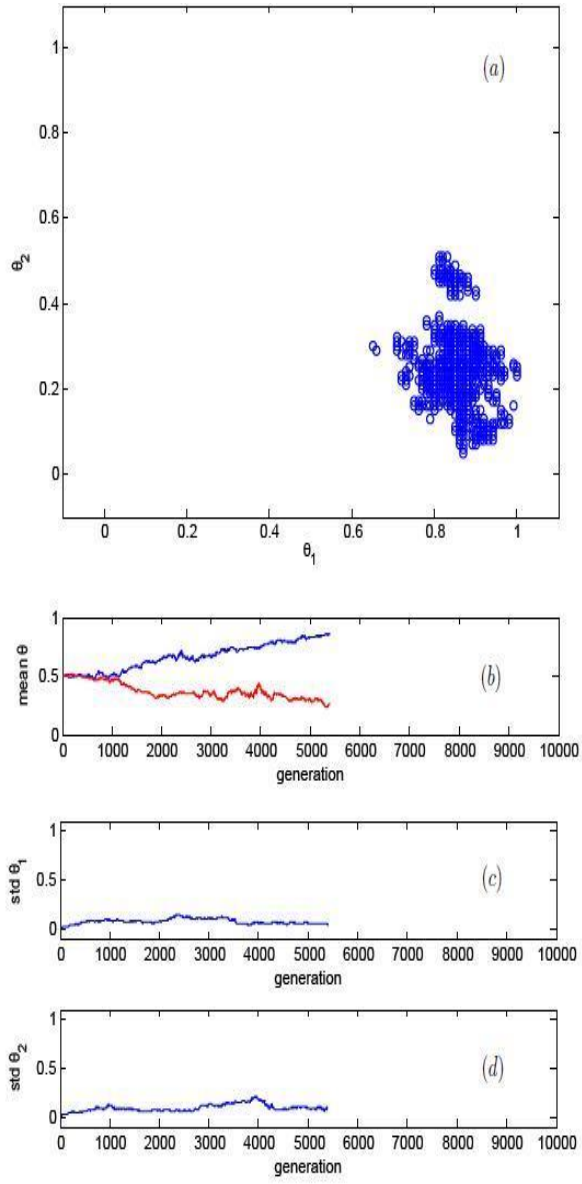

Figure B.2: Example of the graphical Output of the program. The shot was taken after generation 5400. Plot (a) shows the individuals with trait combinations (θ_1, θ_2) at generation 5400. Plot (b) presents the population-wide mean of the two traits θ_1 (blue line), θ_2(red line) as a function of generations (or time). Plot (c) and (d) gives the population-wide standard deviation of trait θ_1 and θ_2, respectively, as a function of generations (or time).

Table B.2: Output parameters

Name	Dimension	Definition
theta1mean	1x *tmax*	mean value of genotype value θ_1
theta2mean	1x*tmax*	mean value of genotype value θ_2
theta1std	1x *tmax*	standard deviation of genotype value θ_1
theta2std	1x*tmax*	standard deviation of genotype value θ_2
nhist	1x*tmax*	array containing the population size each generation
pophist	mx4	matrix containing the genotype values and subpopulation size every 100 generations

```
%  RessourceCompetitionumwandlung(input)
%  Function that simulates the evolution of a population in a
%  variable environment following the model described in
%  Chapter 2.
%  A description of this function can be found in my diploma thesis.

%
% Input arguments:
%

% pop (mx3 matirx): Matrix containing in each line the initial
% genotypic values [theta1 theta2 K] where theta1 and theta2 are
% the genotype values and K is the number of population size having
% this genotype.
% The number of rows is the number of different subpopulations with
% different genotype values that are present in the initial population.

% tmax: Number of generations the simulation runs.

% mPtheta1, mPtheta2: Are the mutation probabilities in
% theta1/theta2.

% mS: Mutational stepsize in theta1/theta2. Stepsize in theta1/theta2
% is always equal.

% r (1x2 array): array containing the growth rates for resource 1 and
% resource 2 respectively

% d (1x2 array): array containing the death rates for resource 1 and
% resource 2 respectively

% c (1x2 array): array containing the conversion efficiency for
```

```
% resource 1 and resource 2 respectively

% g: the death rate of consumer

% ------------------------------------
% simulation. parameter:
% ------------------------------------

% initial values of population size with two trait values:
pop=input.pop;

% maximum genereation steps:
tmax=input.tmax;

% mutation rate of theta1/theta2:
mPtheta1=input.mPtheta1;
mPtheta2=input.mPtheta2;

% mutationstep size:
mS=input.mS;

% ------------------------------------
% model parameters:
% ------------------------------------

% growth rate resource1/resource2:
r=input.r;

% death rate resource1/resource2:
d=input.d;

% death rate consumer
g=input.g;

% conversion efficency for resource1/resource2:
c=input.c;


%
% performance functions parameters:
%

thetas=input.thetas;
```

```
alpha=input.alpha;

beta=input.beta;

% curvature of performance function1/performance function2:
gamma=input.gamma;

% interaction term of performance function1/performance function2:
delta=input.delta;

% noplot(optional): supresses graphical output if 1.


%
% Output:
%

% theta1mean, theta2mean: mean value of genotype value theta1/theta2

% nhist (1xtmax): array containing the population size each generation

% pophist (mx4): matrix containing the genotype values, the number of
% individuals carrying these traits of the whole population present
% every 100 generations (theta1 theta2 K tmax/100)


% initialise the variables defining the outcome
theta1mean=zeros();
theta2mean=zeros();
theta1std=zeros();
theta2std=zeros();
nhist=zeros(1,tmax);
pophist=[];

% ------------------------------------
% ------------------------------------

% ------------------------------------
% ------------------------------------


% ------------------------------------
% start the iteration
% ------------------------------------
```

```
   %  from first to tmax generation

for t=1:tmax
    nhist(t)=sum(pop(:,3));
    % calculate mean values of theta1 and theta2
    theta1mean(t)=sum(pop(:,1).*pop(:,3))/nhist(t);
    theta2mean(t)=sum(pop(:,2).*pop(:,3))/nhist(t);
    theta1std(t)=sqrt((1/sum(pop(:,3)))*sum(pop(:,3).*...
            (pop(:,1)-theta1mean(t)).^2));
    theta2std(t)=sqrt((1/sum(pop(:,3)))*sum(pop(:,3).*...
            (pop(:,2)-theta2mean(t)).^2));

    % ------------------------------------
    % Graphical Output
    % ------------------------------------
    % save the whole population in pophist and plot genotype values of
    % individuals of the resident population every 100 generations
    if  t/100==floor(t/100)
        pophist(end+1:(end+size(pop,1)),:)=[pop t*ones(size(pop,1),1)];
        if ~input.noplot
        figure(1);
        % plot of individuals in the two dimensional trait space present
        % each 100th generation
        plot(pop(:,1),pop(:,2),'o')
        axis([-0.1 1.1 -0.1 1.1]);
        xlabel('\theta_1')
        yLabel('\theta_2')
        %timeseries plot of mean of theta1 and theta2
        figure(2)
        subplot(3,1,1)
        plot(1:t,theta1mean);
        hold on
        plot(1:t,theta2mean,'r');
        hold off
        xlabel('generation');
        ylabel('mean \theta');
        axis([0  tmax 0 1]);
        drawnow;
        % timeseries plot of standard deviation of theta1
        subplot(3,1,2)
        plot(1:t,theta1std);
        ylabel('std \theta_1');
        xlabel('generation');
        axis([0 tmax -0.1 1.1]);
```

```
        % timeseries plot of standard deviation of theta2
        subplot(3,1,3)
        plot(1:t,theta2std);
        ylabel('std \theta_2');
        xlabel('generation');
        axis([0 tmax -0.1 1.1]);
        end
    end


% -----------------------------------
% Population dynamics
% -----------------------------------

% determine performance values for resource1 and resource2:
 F1=alpha(1,1)+beta(1,1)*(pop(:,1)-thetas)+beta(1,2)*(pop(:,2)-thetas)+...
        1/2*(gamma(1,1)*(pop(:,1)-thetas).^2+gamma(1,2)*...
        (pop(:,2)-thetas).^2+2*delta(1)*(pop(:,1)-thetas).*...
        (pop(:,2)-thetas));
 F2=alpha(1,2)-beta(2,1)*(pop(:,1)-thetas)-beta(2,2)*(pop(:,2)-thetas)+...
        1/2*(gamma(2,1)*(pop(:,1)-thetas).^2+gamma(2,2)*...
        (pop(:,2)-thetas).^2+2*delta(2)*(pop(:,1)-thetas).*...
        (pop(:,2)-thetas));

% sizes of resource 1 and resource 2:
 R1d=r(1,1)/(d(1,1)+sum(pop(:,3).*F1));
 R2d=r(1,2)/(d(1,2)+sum(pop(:,3).*F2));

% fitness function:
 fit=-g+c(1,1)*R1d*F1+c(1,2)*R2d*F2;

% determines how fit each individual is in the next generation (drawn from
 a poisson distribution):
 pop(:,3)=poissrnd(pop(:,3).*exp(fit));


%  Mutations occur:

% generates random numbers from the binomial distribution with
% parameters specified by the number genotypes, and probability
% of success for a mutation rate

% mutation in theta1 (drawn from a binomial distribution):
 MutTheta1=binornd(pop(:,3),mPtheta1);
```

```
% mutation in theta2 (drawn from a binomial distribution):
 MutTheta2=binornd(pop(:,3),mPtheta2);

% the new population is the old population and mutated individuals
% removed from it:
 pop(:,3)=pop(:,3)-MutTheta1-MutTheta2;



% -----------------------------------
% Mutational process
% -----------------------------------

 %  Produces a vector with the indices of the genotypes (row number
 %  in the genotype matrix) for which at least one mutation occurs:
   Idx_MutTheta1=find(MutTheta1);
   Idx_MutTheta2=find(MutTheta2);


   %  Mutation in MutTheta1:
   %
   %  Mutational step is drawn from binomial distribution.
   %  Values exceeding the bounds are set to the bounds.
   %  Detetermine whether resulting genotype is already present in
   %  population and add it to the subpopulation.
   %  If not create a new entry in the population vector.
   for i=1:length(Idx_MutTheta1)
           for j=1:MutTheta1(Idx_MutTheta1(i))
           Theta1New=min(1,max(0,pop(Idx_MutTheta1(i),1)+...
               sign(rand-0.5)*mS));
           x=find((pop(:,1)==Theta1New).*(pop(:,2)==...
               pop(Idx_MutTheta1(i),2)),1);
                if isempty(x)
                    pop(length(pop)+1,:)=[Theta1New ...
                    pop(Idx_MutTheta1(i),2) 1];
               else
                    pop(x,3)=pop(x,3)+1;
                end

         end
   end

   %  Mutation in MutTheta2:
```

```
    %
    %  same process for MutTheta2
    for i=1:length(Idx_MutTheta2)
            for j=1:MutTheta2(Idx_MutTheta2(i))
            Theta2New=min(1,max(0,pop(Idx_MutTheta2(i),2)+...
                sign(rand-0.5)*mS));
            x=find((pop(:,2)==Theta2New).*...
                (pop(:,1)==pop(Idx_MutTheta2(i),1)),1);
                 if isempty(x)
                     pop(length(pop)+1,:)=[pop(Idx_MutTheta2(i),1)...
                         Theta2New 1];
                else
                     pop(x,3)=pop(x,3)+1;
                 end


            end

    end

    %  Clear genotypes with population size 0 from the population
    %  vector (meaning that no individual has this genotype
    %  combination) and if no individual is left write all died out:
    pop(pop(:,3)<=0,:)=[];
    if length(pop) <=0
        display 'All died out'
        break;
    end

end


end
```

List of Figures

List of Tables

Bibliography

N. Barton, D.E.G.; Briggs, J.A. Eisen, D.B.; Goldstein, and N.H. Patel. *Evolution*. Cold Spring Harbor Laboratory, 2007.

P. M. Butler. Evolution and mammalian dental morphology. *Journal De Biologie Buccale*, 11(4):285–302, 1983.

N.A. Campbell. *Biologie*. Spektrum Lehrbuch, 1997.

J. L. Cisne. Evolution of world fauna of aquatic free-living arthropods. *Evolution*, 28(3):337–366, 1974.

C. De Mazancourt and U. Dieckmann. Trade-off geometries and frequency dependent selection. *The American Naturalist*, 164(6):765–778, December 2004. ISSN 00030147. URL `http://www.jstor.org/stable/10.1086/424762`.

U. Dieckmann and R. Law. The dynamical theory of coevolution: A derivation from stochastic ecological processes. *Journal of Mathematical Biology*, 34(5-6):579–612, 1996.

O. Diekmann. A beginner's guide to adaptive dynamics. *Mathematical Modelling of Population Dynamics Banach Center Publications, Institute of Mathematics Polish Academy of Sciences Warszawa 2004*, 63, 2004.

C. Espinosa-Soto and A. Wagner. Specialization can drive the evolution of modularity. *PLoS Comput Biol*, 6(3):e1000719, 03 2010. doi: 10.1371/journal.pcbi.1000719.

S. A. H. Geritz, J. A. J. Metz, E. Kisdi, and G. Meszena. Dynamics of adaptation and evolutionary branching. *Physical Review Letters*, 78(10): 2024–2027, 1997.

S. A. H. Geritz, E. Kisdi, G. Meszena, and J. A. J. Metz. Evolutionarily singular strategies and the adaptive growth and branching of the evolutionary tree. *Evolutionary Ecology*, 12(1):35–57, 1998.

J. Hofbauer and K. Sigmund. *Evolutionary Games and Population Dynamics*. Cambridge University Press, 1998.

D. L. Kirk. A twelve-step program for evolving multicellularity and a division of labor. *Bioessays*, 27(3):299–310, March 2005. doi: 10.1002/bies.20197.

E. Kisdi. Trade-off geometries and the adaptive dynamics of two co-evolving species. *Evolutionary Ecology Research*, 8(6):959–973, 2006.

R. Law. Optimal life histories under age-specific predation. *American Naturalist*, 114(3):399–417, 1979.

O. Leimar. The evolution of phenotypic polymorphism: Randomized strategies versus evolutionary branching. *The American Naturalist*, 165(6):669–681, June 2005. ISSN 00030147. URL `http://www.jstor.org/stable/3473518`.

O. Leimar. Multidimensional convergence stability. *Evolutionary Ecology Research*, 11(2):191–208, 2009.

J. L. Ma and S. A. Levin. The evolution of resource adaptation: How generalist and specialist consumers evolve. *Bulletin of Mathematical Biology*, 68(5):1111–1123, 2006. doi: 10.1007/s11538-006-9096-6.

J. A. J. Metz, R. M. Nisbet, and S. A. H. Geritz. How should we define fitness for general ecological scenarios. *Trends In Ecology & Evolution*, 7 (6):198–202, 1992.

J. A. J. Metz, S. A. Geritz, G. Meszena, van Heerwaarden, and J.S. G. Jacobs. Adaptive dynamics: A geometrical study of the consequences of nearly faithful reproduction. *van Strien SJ, Verduyn Lunel SM (eds): Stochastic and Spatial Structures of Dynamical Systems, Proceedings of the Royal Dutch Academy of Science (KNAW Verhandelingen), North Holland, Amsterdam*, pages pp. 183–231, 1996. URL `http://www.iiasa.ac.at/Research/ADN/Series.html`.

C. Rueffler and G. Wagner. Evolution of functional specialization and division of labor. *Proceedings of the National Academy of the Sciences of the U.S.A.*, in rev.

C. Rueffler, T. J. M. Van Dooren, and J. A. J. Metz. Adaptive walks on changing landscapes: Levins' approach extended. *Theoretical Population Biology*, 65(2):165–178, March 2004. doi: 10.1016/j.tpb.2003.10.001.

C. Rueffler, T. J. M. Van Dooren, O. Leimar, and P. A. Abrams. Disruptive selection and then what? *Trends In Ecology & Evolution*, 21(5):238–245, 2006a. doi: 10.1016/j.tree.2006.03.003.

C. Rueffler, T. J. M. Van Dooren, and J. A. J. Metz. The evolution of resource specialization through frequency-dependent and frequency-independent mechanisms. *American Naturalist*, 167(1):81–93, 2006b.

D. Schluter. Adaptive radiation in sticklebacks - trade-offs in feeding performance and growth. *Ecology*, 76(1):82–90, January 1995. doi: 10.2307/1940633.

H. Svardal. Evolution of phenotype determination - stochastic simulations of adaptation in time-varying environments. Master's thesis, Vienna University of Technology, Austria, 2008.

T. J. M. Van Dooren, M. Durinx, and I. Demon. Sexual dimorphism or evolutionary branching? *Evolutionary Ecology Research*, 6(6):857–871, 2004.

E. O. Wilson. Caste and division of labor in leaf-cutter ants (hymenoptera, formicidae, atta) .1. the overall pattern in atta-sexdens. *Behavioral Ecology and Sociobiology*, 7(2):143–156, 1980.

J. Zu, K. Wang, and M. Mimura. Evolutionary branching and evolutionarily stable coexistence of predator species: Critical function analysis. *Mathematical Biosciences*, In Press, Uncorrected Proof:–, 2011. ISSN 0025-5564. doi: DOI: 10.1016/j.mbs.2011.03.007.

Curriculum Vitae

Personal Data

Name:	Helene Camilla Weigang
Place of Birth:	Vienna, Austria
Date of Birth:	01.April 1988
Nationality:	Austrian

Education

1994 - 1998	Elementary school Diesterweggasse, 1140 Vienna
1998 - 2006	Secondary school Wenzgasse, 1130 Vienna
20.06.2006	Matura (High school degree)
WS 06/07-SS 11	Studies at the University of Vienna, Mathematics (Diploma)
SS 2009	Studies abroad at the Universitat Autonoma de Barcelona
WS 06/07- SS 09	Studies at the University of Vienna, Pharmacy (Diploma) discontinued

Workshops Participated

March 2011:	European Science Foundation - Frontiers of Speciation Research, Winter School, Eco-evolutionary Modeling of Speciation. Absiko, Sweden
June 2011:	Kellogg Biological Station - Summer Educational Program, Enhancing Linkages between Mathematics and Ecology: Adaptive Dynamics. Kalamazoo, USA